Semiannual Technical Summary

Seismic Discrimination

31 December 1970

Prepared for the Advanced Research Projects Agency
under Electronic Systems Division Contract F19628-70-C-0230 by

Lincoln Laboratory

MASSACHUSETTS INSTITUTE OF TECHNOLOGY

Lexington, Massachusetts

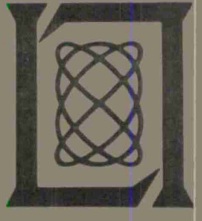

MASSACHUSETTS INSTITUTE OF TECHNOLOGY

LINCOLN LABORATORY

SEISMIC DISCRIMINATION

SEMIANNUAL TECHNICAL SUMMARY REPORT
TO THE
ADVANCED RESEARCH PROJECTS AGENCY

1 JULY – 31 DECEMBER 1970

ISSUED 4 FEBRUARY 1971

LEXINGTON MASSACHUSETTS

The work reported in this document was performed at Lincoln Laboratory, a center for research operated by Massachusetts Institute of Technology. This research is a part of Project Vela Uniform, which is sponsored by the Advanced Research Projects Agency of the Department of Defense under Air Force Contract F19628-70-C-0230 (ARPA Order 512). Part of the work reported herein is supported by Air Force Contract AF 49(638)-1763 with Massachusetts Institute of Technology.

ABSTRACT

Research on source characteristics, propagation path effects and array processing is reported. The long-period characteristics of explosions are examined and tested against theoretical models. Short period worldwide data are used for a network study of a set of Eastern Kazakh events. A new computer program is being used to trace rays through heterogeneous structures. A detailed study of a Chinese event is given with particular reference to the impact that subsurface structure has on different discriminant tests. The spectraforming process is described and its impact on discrimination discussed. New facilities and the daily Lincoln bulletin are described.

Accepted for the Air Force
Joseph R. Waterman, Lt. Col., USAF
Chief, Lincoln Laboratory Project Office

CONTENTS

SUMMARY

This is the fourteenth Semiannual Summary of the Seismic Discrimination Group of Lincoln Laboratory. In order to establish the technical basis for any proposed arms control agreement banning underground nuclear explosions, we are pursuing research connected with the nature of explosions and earthquakes, the propagation path from source to receiver and methods of data analysis at the receiver. In particular, much of our research is centered on LASA, the Large Aperture Seismic Array in Montana. This report is divided into four sections, dealing with: source characteristics; propagation path; array processing research; and facilities in the Laboratory which support the research.

In Section I we report on spectral analysis of surface wave data from explosions at the Nevada Test Site. A wide range of explosions has been analyzed in order to see if spectral characteristics vary with magnitude and if standard models of the explosive source adequately describe the radiation at long periods. A large composite diagram of all the data is presented along with theoretical predictions. A discussion of energy partitioning is given and it is concluded that less than 1 percent of the available elastic energy at long periods goes into surface waves. In another study, short period observations of explosions from seismic rays which have been reflected off the inner core are presented. These signals are very little encumbered by interfering signals and the source characteristics that they suggest are unusual, calling for pulses of equal and opposite polarity 2 sec apart. This is discussed in the light of present models of explosive displacement potentials. A multi-array study of Eastern Kazakh events of a range of magnitudes is discussed. Use of theoretical explosion models to construct transfer functions from one magnitude to another and the calculation of experimental transfer functions from the data allows us to compare different explosive source models. We also note that there is a marked difference in signal character from array to array, indicating some considerable variability in radiation characteristics for different directions.

In Section II we report several studies on the propagation path. Use of the high-resolution technique for analysis of surface waves having a 40-sec period reveals multipath phenomena almost as complex as earlier studies at higher frequencies had revealed. It is again possible to associate these multipath signals with reflections from continental margins and tectonic features. In addition to multipath Rayleigh waves, it is possible to find very-long-period body waves in the coda. Many of these have been identified as of the general type $(PS)_n$ where n is of the order of six. The ray-tracing program, described briefly in the last Semiannual Summary, is now being used to explore the implications of lateral inhomogeneities in the earth. In particular, realistic models for underthrust plates have been used and the powerful effect of inhomogeneities in producing shadows and high-amplitude regions is obvious. P-waves from two earthquakes practically at the same location and PcP from the same events recorded at LASA are displayed side by side to reveal the effect that the Aleutians plate has on introducing disturbances into the waveform of P-waves. A Chinese event has raised some important questions for discrimination and these are discussed with respect to P-wave propagation in the earth. The event appears to have a very clear depth phase, pP, associated with it. It, however, would be classed as a possible explosion by the M_s:m_b criterion. Insights into the upper mantle structure beneath China can be drawn from this event and are important for discrimination. An

unusual opportunity to make a direct measurement of the earth's Q was possible with the installation of near-shot seismometers for the nuclear test, Boxcar. Teleseismic observations of the signal at NORSAR were combined with the near-source observations to obtain a mean Q for the path of about 2000.

Section III deals with array processing research. A description is given of recent developments in the spectraforming method of processing partially coherent seismic data. So far it has been clearly demonstrated that averaged spectral information from selected sensors in LASA is greatly superior to the spectrum of a time-domain beam from the same sensors. In particular, high frequencies are very well preserved by spectraforming. On the other hand, the signal-to-noise improvement of time-domain beamforming is not available to the spectraform. The method is discussed with particular reference to the use of higher frequencies for discrimination. A further contribution considers the capabilities of a new estimator of the energy density spectrum. This estimator uses noise statistics and is able to yield a signal-to-noise ratio gain of 3 to 9 dB over the conventional spectraform process. A study has been completed of the ability of LASA to detect signals in the presence of interfering signals. In particular, Rayleigh waves from one event are searched for in the main wavetrain and the coda of another event. The long duration of the coda frequently makes it the dominant feature in masking events, so coda statistics have also been gathered. It is concluded that a signal 6 dB below the interfering signal can be correctly identified. The opportunity at LASA to sample a larger portion of the seismic wave field than an individual seismic station can enables us to look very carefully at what seismological statements, particularly with regard to amplitude, are tenable. A study of P and PcP amplitudes has been made and shows the extent of scatter and how much of this is attributable to source structure. It is concluded that the PcP/P ratio is a difficult figure to extract from individual observations.

In Section IV we note new developments in the Laboratory's facilities. The Analysis Console has been our major research tool for studying seismic data and continues to provide excellent service in making seismic data from any digital source rapidly accessible. Improvements are noted and it is now possible to study several arrays or several events simultaneously. Our seismic bulletin provides a daily coverage of seismic activity in the teleseismic region to LASA. Its capabilities are described here in terms of location threshold – the level at which an event can be seen clearly enough to allow a location to be performed.

D. Davies

GLOSSARY

ALPA	Alaskan Long Period Array
LASA	Large Aperture Seismic Array, Billings, Montana
NORSAR	Norwegian Seismic Array
NTS	Nevada Test Site
SATS	Semiannual Technical Summary
TFO	Tonto Forest Seismological Observatory
UK	United Kingdom
USCGS	United States Coast and Geodetic Survey
VESPA	Velocity Spectral Analysis

SEISMIC DISCRIMINATION

I. SOURCE CHARACTERISTICS

A. SCALED RAYLEIGH WAVE SPECTRA FROM EXPLOSIONS

We have conducted a study of the spectra of the vertical component of Rayleigh wave motion from some 25 NTS explosions recorded at LASA. The purpose of the study is to test various proposed models of the shape of the explosive source spectrum, to examine the variability of these spectra due to small changes in location of the source and recording site, and to observe the scaling of the spectra as a function of yield and medium. We have used up to four LASA sites to study each event. Within the experiment we have attempted to keep all processing parameters (such as window length, sampling interval, position of the wavetrain within the window, and tapering procedure) constant so that any contrast or similarities between events or seismometer sites can be considered reliable.

The central question we address concerns the shape of the amplitude spectrum of explosions at long periods. Is it flat, or do the amplitudes decrease with increasing period? A flat spectrum from, say, 10 to 100 sec is predicted by Haskell's[1] model and by that of a buried spherical cavity with a pressure step function applied at the cavity wall. Source spectral amplitudes which decrease with increasing period can be modeled by a buried cavity with a broad pressure pulse, of the form $te^{-\eta t}$ for $t > 0$, say, applied to the cavity wall. The question is not purely an academic one since a long-period spectral ratio is suggested as a discriminant between earthquakes and explosions by Molnar, et al.,[2] and the shape of the long-period spectrum is used in determining focal depth (thus acting as a discriminant except for very shallow earthquakes) by Tsai and Aki.[3]

Figure I-1 shows the observed amplitude spectra, corrected for instrument response, from eight explosions recorded at LASA site D1. At the top of this figure are two curves computed to be the Rayleigh wave amplitude spectrum at LASA from NTS. Curve 1 is based on a step-function pressure variation, and curve 2 is based on the broad pulse $te^{-\eta t}$ where $\eta = 1$. The Rayleigh wave transfer function was taken from Toksöz, et al.[4] (their Fig. 9) and closely approximates that computed by Tsai and Aki for a Gutenberg continental earth model (their Fig. 2). Here a Q_R of 400 was assumed at all frequencies.

The point of Fig. I-1 is that it is difficult, given this fairly representative sample of our data, to favor one source spectral model over another. The larger explosions seem to be better represented by curve 1, while the smaller ones are more closely delineated by curve 2. If this effect is real, the conclusion is that (as far as surface waves are concerned) the larger explosions behave as if a step-function pressure pulse is applied to the cavity wall and a decaying pressure pulse is appropriate for smaller explosions. These observed spectra do tend to confirm the result of Tsai and Aki,[3] that the monotonically decreasing nature of observed spectra from 10 to 30 sec is indicative of an explosive source at a shallow focal depth. Minima observed near 0.05 Hz in the spectra of events Hutch and Torrido are not observed at other LASA sites and must be a local effect.

TABLE I-1
AN ESTIMATE OF RAYLEIGH WAVE ENERGY IN NTS EXPLOSIONS

Event	Announced Yield[7] (kt)	Energy (ergs)
Greeley	825	5.9×10^{16}
Boxcar	1200	1.1×10^{17}
Jorum	–	1.0×10^{17}
Benham	1100	8.0×10^{16}
Pipkin	–	6.2×10^{14}
Purse	–	1.4×10^{15}

TABLE I-2
YIELD ESTIMATES OF NTS EXPLOSIONS

Event	Announced Yield[7] (kt)	Estimated Yield (kt)
Greeley	825	860
Benham	1100	1000
Boxcar	1200	Reference event
Jorum	–	1100
Pipkin	–	90
Purse	–	130

Superimposed on the explosion spectrum are the effects of strain energy release due to a prestressed state of the medium. A theory outlining this phenomenon and evidence to support it is given by Archambeau and Sammis.[5] In the case of Bilby, the NTS explosion they discuss, LASA lies on a node of the Rayleigh wave radiation due to tectonic strain release. It might be argued then that LASA lies in a direction from NTS which allows it to look more precisely at the explosion radiation alone. There is some evidence that this is not generally the case. Figure I-2 shows seismograms of the long-period vertical seismometer at site E1 from three large explosions. In each case, the left-hand margin is at one minute after the event origin time. A long-period motion arrives coincidentally with P_n and appears to be in phase for all the events. However, after reducing the gain by a factor of 16, we observe that the Rayleigh waves from Boxcar and Benham, which are very similar and in phase, are π out of phase with those of Greeley. This phenomenon shown by Greeley has been observed at other stations by Toksöz (personal communication). Comparison with the Rayleigh waves from other, smaller, NTS explosions shows that it is indeed Greeley that is out of phase with the majority. This phenomenon may be due to some complicated pattern of tectonic strain release. However, such a release did not drastically change the shape of the spectrum nor, as will be shown, the surface wave energy of this 825 kt explosion compared with other megaton-sized events nearby (see Fig. I-1).

Finally, we have attempted to estimate the energy in the Rayleigh waves at LASA by adapting the method described by Båth[6] to the frequency domain. Here, using only the events on Pahute Mesa and averaging over three LASA sites, we estimate the total energy in Rayleigh waves in the band 0.03 to 0.1 Hz as in Table I-1. Now, given an initial amount of explosive energy in terms of yield (E_w), a certain percentage will go into the elastic wave field (E_α), a percentage of E_α will be in the long-period portion of the spectrum (E_{LP}) and a percentage of E_{LP} will be present in the Rayleigh waves (E_R). For various media, Haskell[1] has predicted E_α/E_w and his theory allows us to compute E_{LP}/E_α. Because of the shape of the explosion spectrum, E_{LP}/E_α is not a constant, but is a function of yield. Haskell's model predicts for tuff that $E_{LP}/E_w = 5.0 \times 10^{-8} W$ where W is in kilotons. Thus for Boxcar, where $E_w \approx 5 \times 10^{23}$ ergs, $E_{LP} = 3 \times 10^{19}$ ergs and our measurements indicate that $E_R/E_{LP} \approx 10^{17}/3 \times 10^{19}$ which is a fraction of 1 percent. The conclusion is that of the elastic energy available in the long-period band of the explosion spectrum, less than 1 percent of it is radiated by the fundamental mode Rayleigh wave within this rather narrow frequency band.

It is the case for both models discussed earlier that the energy in the long-period band varies as W^2. Since all the events in Table I-1 were detonated at about the same location, we should be able to estimate the yield of five of the explosions based on the measured energy and announced yield of the sixth. Using Boxcar as a reference event, such estimates are given in Table I-2. This table points up the difficulty with the Greeley explosion. The phenomenon that reversed the Rayleigh waves of Greeley with respect to Boxcar and Benham apparently did not alter the relative energy content of this phase compared to the larger events.

J. R. Filson
L. Lande

B. SEISMIC SOURCE FUNCTIONS FROM PKiKP

The detailed short-period characteristics of any seismic event, whether explosion or earthquake, are not necessarily well represented by the teleseismic body-wave signal. Even an explosion over a relatively uniform crust and upper mantle produces a wide variety of signals at seismometers at various azimuths and distances. When an event occurs in a region which is strongly laterally inhomogeneous, the variation in P-wave characteristics becomes much more severe, as was shown in the Longshot study in the last SATS. Much of the variation in P-wave character can be attributed to shadowing and multipathing arising from plate structure, triplication of travel time curves, passage of rays through caustics and variable amounts of time spent by rays in low Q regions of the mantle.

It is clearly desirable to attempt to get a more reliable picture of the compressional radiation near the source than can be inferred from teleseismic P-waves. An interesting way in which we have attempted to do this is by use of the phase reflecting off the inner core (PKiKP). This phase, although regularly seen at great distances, was only recently found reliably at short distances (Δ = 20° to 40°) by Engdahl, et al.[8] An array is necessary to identify the phase because it arrives about 17 min after the event, at a time when surface wave energy is generally high. This phase is barely seen at individual seismometers and the power of the whole array is necessary to pull out the signal. Figure I-3 demonstrates this capability.

The signal is remarkably clear and the $dT/d\Delta$ is close to that predicted by Engdahl, et al.[8] The travel time agrees to within 1 sec with theirs. It is important to note that there has been no filtering at all of these data between recording at LASA and this display. It is thus as broad band as is available with short-period seismometers. The indications are that reflections from the inner core boundary, small though they be, are sharp pulses consistent with reflection without a phase shift from a very sharp boundary. The ray travels nearly vertically through the upper mantle and thus has the shortest time of any teleseismic P-phase in postulated low Q zones in the upper mantle. This, too, adds to the possibility of the phase being a relatively undistorted view of the source.

Figure I-4 is a display of several PKiKP phases from underground explosions in Nevada, recorded at LASA. They have all been produced by selecting only those subarrays which showed the phase above the background and by appropriate delay and sum operations.

The record from Faultless is the most clear, but at the same time it is well known that Faultless produced extensive near-source surface-rupturing on detonation, so we are probably looking at an explosion and an earthquake or even a series of earthquakes.

The record from Boxcar is intriguing. Although the first motion appears to be downward, a trained analyst, used to allowing for instrumental response, would report the signal as starting upward. Note that in the first 1.5 sec this isolated pulse appears to integrate to a finite area, a feature which inertial seismometers cannot display over any length of time, owing to their zero response at DC. The second pulse is an exact replica, inverted, of the first and is followed by a relatively insignificant coda. A somewhat comparable observation of two pulses was made by Engdahl, et al., studying Benham and Jorum. Examples of the signal from Purse, Benham, and Jorum are also given in Fig. I-4. It will be seen that, in the absence of band-pass

filtering, it is not possible to talk about these phases as having an amplitude, in the sense normally used in seismology, of half the maximum peak-to-peak signal. Caution should thus be exercised in comparing amplitudes of PKiKP with those of other phases where at least two adjacent peaks of opposite polarity are almost invariably seen.

What causes this double pulse? Why is the signal so unusual in character? The signal character appears to be associated with a very high Q path and a complete lack of multipathing. It bears a very strong resemblance to some of the theoretical signals calculated by Carpenter,[9] which are relatively difficult to observe among teleseismic P-waves owing to the confusions of multiple paths and (at $\Delta > 80°$) core interference. There is a problem of the apparent absence of pP. These shots are usually buried at a depth of about 1 km and located in tuff or hard rock. It thus seems unreasonable that the second pulse (e.g., for Boxcar) is pP, as the pP-P time interval can hardly be more than 1 sec. Absence of pP might reasonably be associated with the impossibility of elastic radiation passing through the highly fractured explosion zone in any coherent fashion. This leaves unanswered the problem of the second pulse. Since the interval between the two pulses is slightly variable and since earthquakes studied have not generally revealed similar features, it seems impossible to explain the effect by inner core structure. Reduced displacement potential measurements of much smaller explosions have indicated that the potential, the derivative of which is proportional to signal amplitude, has a time function which is approximately a step on which an impulse is superimposed. The size of the impulse, based on a very small sample of explosions, is strongly dependent on the medium in which the shot was fired, but appears to be most pronounced for salt, granite and alluvium, and relatively insignificant for tuff. Figure I-5 shows such a reduced displacement potential.[10] However, results up to the present have been restricted to observations from relatively small explosions (a few kilotons). The reduced displacement potential displayed seems to have just as steep a negative gradient, with respect to time, on the tail of the impulse as it has a positive gradient on the front end. At 5 kt the peak negative gradient occurs typically 0.15 sec after the positive peak. Cube root scaling of yield suggests that the time scale for explosions with yields in the vicinity of a megaton should increase about a factor of six.

It is thus reasonable to associate the second pulse with the return of the overshoot in the reduced displacement potential. Further work on this feature is being pursued in order to try and relate it to different yields and source media and to find the implications for teleseismic discrimination at lower magnitudes. The richness in energy, on long-period instrument recordings of P-waves from explosions, that has been observed at periods of about 2 sec by Molnar and Wyss, et al. (personal communications) seems to have an explanation in terms of this double pulsed source function.

D. Davies

C. USE OF SHORT PERIOD DATA TO EXAMINE EXPLOSIVE SOURCE CHARACTERISTICS

The study of short period source characteristics from presumed explosions in Eastern Kazakh has been continued. Previously,[11] transfer functions, to shape low to high magnitude P-waves recorded at LASA, were interpreted in terms of source functions, using Blake's solution[12] for compressional waves radiated by a spherical cavity excited by a step function of

pressure. These calculations have been refined and extended to the world-wide arrays used by Filson[11, 13] in a previous study of the same data. The arrays are the following: GBA (Gauribidanur, India); OONW (Oslo, Norway); YKA (Yellowknife, Canada); LASA (Billings, Montana); and WRA (Warramunga, Australia).

Figure I-6 shows the steered beams of the four events recorded at the arrays. At LASA, the subarray sum trace of F3 is shown to illustrate the beams of arrays of comparable aperture. Event 5 is plotted with unit amplitude on each array (the other events being scaled down to show their correct amplitudes relative to event 5).

Transfer functions $R_{i5}(t)$ were computed to shape event i to event 5 at each array. Since the four events have common epicenters within $\sim 0.5°$ circle, the transmission path effects of each event to a given array are equal. In the frequency domain, such transmission path effects divide out and we obtain

$$R_{ij}(w) = E_j(w)/E_i(w) = S_j(w)/S_i(w) \tag{1}$$

where $E_i(w)$ and $S_i(w)$ are, respectively, Fourier transforms of the recorded P-wave and the source function (including burial depth effect) of event i.

Time domain transfer functions $R_{15}(t)$, $R_{25}(t)$ and $R_{45}(t)$ for the available data at each array are displayed in Fig. I-7. It is clear from Figs. I-6 and I-7 that the four events do not have isotropic source radiation patterns. For example, $R_{45}(t)$ seems consistent on all arrays, suggesting that events 4 and 5 have similar radiation patterns, however complex. $R_{15}(t)$, however, varies considerably from array to array, implying that events 1 and 5 have different radiation patterns.

Two isotropic source models for explosions are those of Haskell[1] and Blake.[12] For a granitic source medium, Haskell's reduced displacement potential for 5-kt yield can be scaled to any magnitude using a suitable magnitude-yield relationship. For a hard rock source region, the yield, Y (kilotons), can be approximated[13, 14] by the formula

$$m_b = 3.8 + \log_{10} Y \quad . \tag{2}$$

For Blake's solution, the radius in meters, a, of an equivalent elastic cavity is required. This is estimated[14] by

$$a = 100 Y^{1/3} \quad . \tag{3}$$

Using the LASA magnitudes of the four events, one can obtain the set of a_i and Y_i given in Table I-3. From these values, the particle velocity curves for the four events were calculated using each model and are shown in Fig. I-8.

Theoretical transfer functions to shape low to high magnitude source functions were computed for each model. These are superposed on the LASA transfer functions in Fig. I-9. The overall amplitude and shape of the transfer functions for Blake's model appear to fit the LASA data better than those for Haskell's model.

Figure I-10 shows the frequency response of the observed LASA transfer functions. This demonstrates the degradation of high frequencies with increasing magnitude, predicted by all explosion source models.

TABLE I-3
ESTIMATES OF YIELD AND CAVITY RADIUS FROM LASA MAGNITUDES

Event	m_b (LASA)	Yield (kt)	Cavity Radius (m)
1	5.4	40	341
2	5.6	63	398
4	5.8	100	464
5	6.1	199	584

Isotropic source models, of course, cannot explain the world-wide array data. The largest unknown factor is the depth of burial of each presumed explosion. Numerical studies of the coupling effect between explosion cavities and the free surface should be pursued as the next step in understanding teleseismic radiation from explosions.

C. W. Frasier

D. SOURCE CHARACTERISTICS OF SMALL EARTHQUAKES AND EXPLOSIONS

An investigation of the regional seismicity near LASA has been initiated with the eventual goal of comparing the source characteristics of small regional earthquakes and explosions. The several chemical explosions near LASA, detonated for a U.S. Geological Survey (refraction survey) in the fall of 1968, provide an adequate explosion population for such a study. The LASA bulletin routinely lists events with epicenters within about 12° of LASA as regional. A spot check of the bulletin for 1967-68 indicated an average of slightly less than half a dozen regional events per day. Of the several regional events for which high-rate (i.e., all sensors) data tapes have been examined, the two most promising events occurred on 28 December 1966 at 0929 GMT and on 2 July 1967 at 0853 GMT, respectively. Preliminary epicenters for these events are about 80 km southwest of the F3 subarray and 150 km south of the E3 subarray, respectively.

W. H. Bakun

REFERENCES

1. N. A. Haskell, "Analytic Approximation for Elastic Radiation from a Contained Underground Explosion," J. Geophys. Res. 72, 2583-2587 (1969).
2. P. Molnar, J. Savino, L. R. Sykes, R. C. Lieberman, G. Hade and P. W. Pomeroy, "Small Earthquakes and Explosions in Western North America Recorded by New High Gain, Long Period Seismographs," Nature 224, 1266-1273 (1969).
3. Y-B Tsai and K. Aki, "Amplitude Spectra of Surface Waves from Small Earthquakes and Underground Nuclear Explosions," in press (1970).
4. M. N. Toksöz, A. Ben-Menahem and D. G. Harkrider, "Determination of Source Parameters of Explosions and Earthquakes by Amplitude Equalization of Seismic Surface Waves, Part 1," J. Geophys. Res. 69, 4355-4366 (1964).
5. C. Archambeau and C. Sammis, "Seismic Radiation from Explosions in Prestressed Media and the Measurement of Tectonic Stress in the Earth," Reviews of Geophysics and Space Physics 8, 473-500 (August 1970).
6. M. Båth, "Earthquake Energy and Magnitude," in Physics and Chemistry of the Earth, Vol. 7 (Pergamon Press, New York, 1966), pp. 115-165.
7. G. Higgins, "Summary of Nuclear Explosion Data for Underground Engineering Applications," UCRL Report No. 50853, Lawrence Radiation Laboratory, University of California (April 1970).
8. E. R. Engdahl, E. A. Flinn and C. F. Romney, "Seismic Waves Reflected from the Earth's Inner Core," Nature 228, 852-853 (1970).
9. E. W. Carpenter, "Teleseismic Signals Calculated for Underground, Underwater and Atmospheric Explosions," Geophysics 32, 17-31 (1967).
10. J. E. Roberts, "Spectral Composition of Seismic Source Functions Associated with some Representative Nuclear Detonations," UCRL Report No. 50763, Lawrence Radiation Laboratory, University of California (October 1969).
11. Seismic Discrimination, Semiannual Technical Summary Report to the Advanced Research Projects Agency, Lincoln Laboratory, M. I. T. (30 June 1970), Sec. I-A, DDC AD-710613.
12. F. G. Blake, "Spherical Wave Propagation in Solid Media," J. Acoust. Soc. Am. 24, 211-215 (1951).
13. J. R. Filson, "On Estimating Explosive Source Parameters at Teleseismic Distances," Technical Note 1970-9, Lincoln Laboratory, M. I. T. (8 July 1970), DDC AD-709767.
14. D. Davies (rapporteur), Seismic Methods for Monitoring Underground Explosions (SIPRI, Stockholm, 1968).

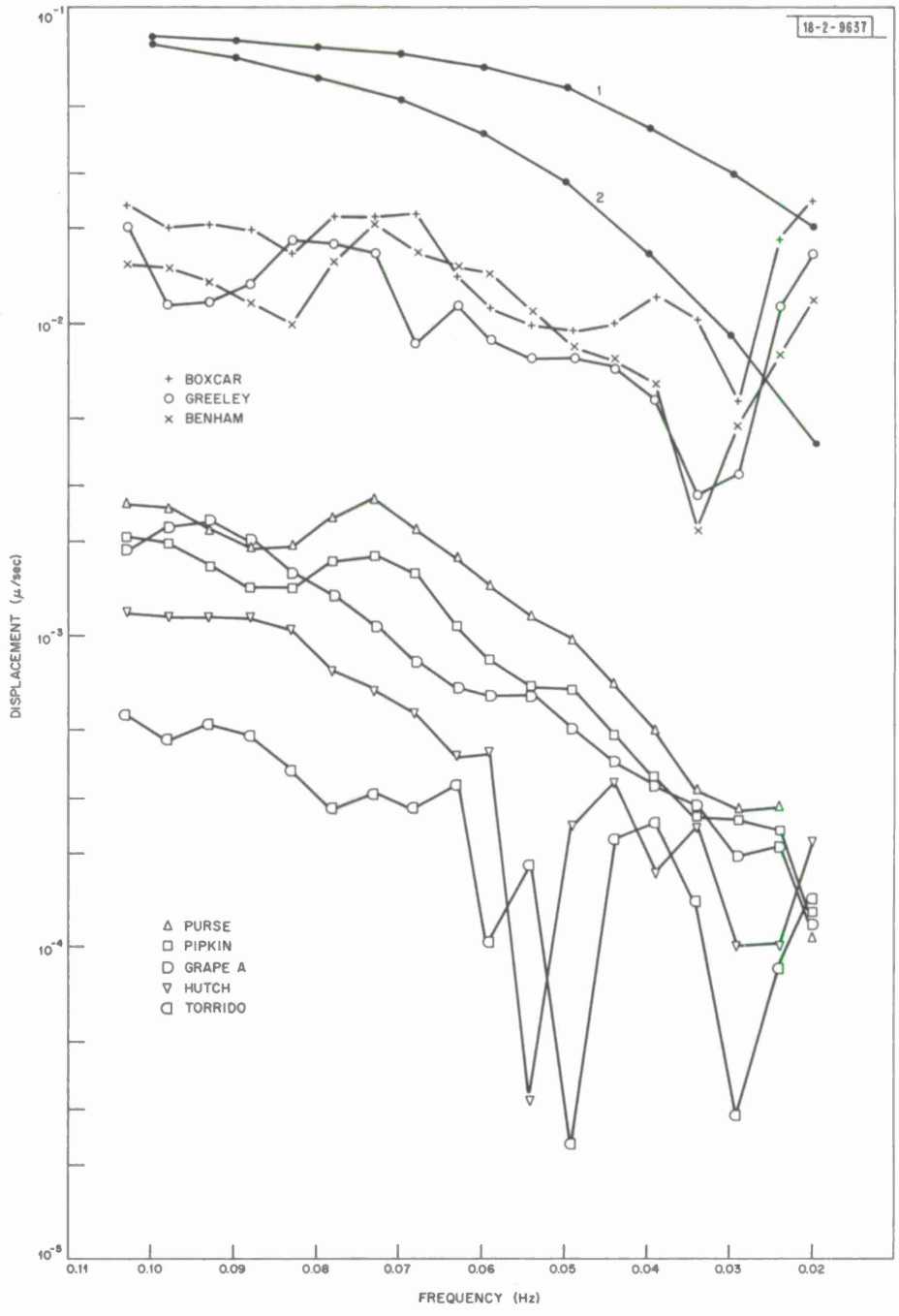

Fig. I-1. Curves 1 and 2 are theoretical predictions of the amplitude spectrum of the vertical component of Rayleigh wave motion at LASA from explosive sources at NTS. The source pressure variation was modeled by a step-function when computing curve 1 and by a decaying pulse in the case of curve 2. Plotted are the scaled amplitude spectra due to the vertical component of Rayleigh wave motion (corrected for instrument response) at LASA site D1 from various NTS explosions.

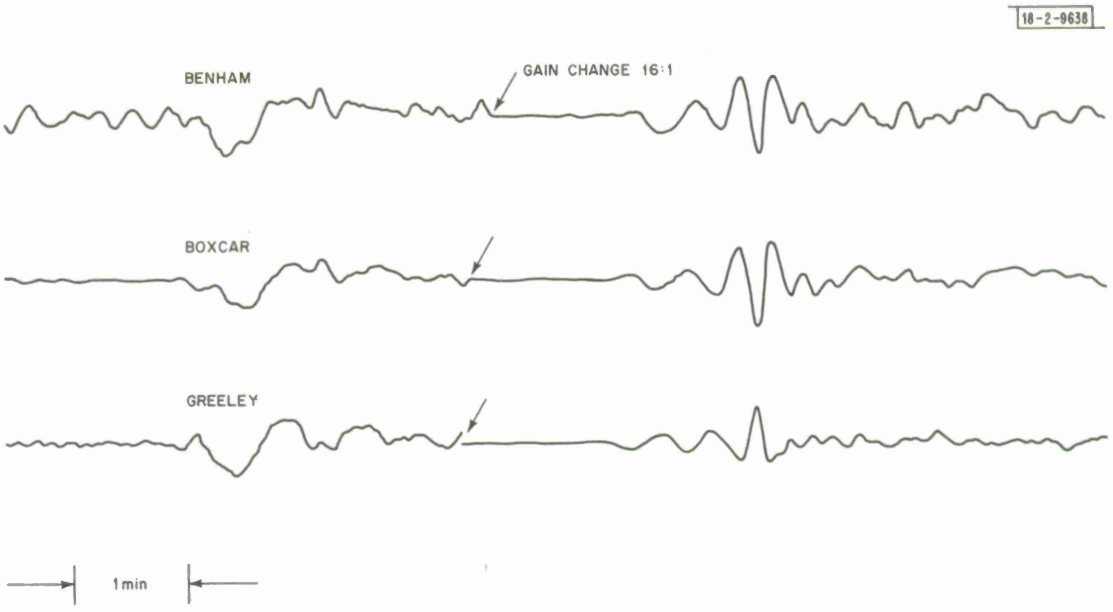

Fig. I-2. Vertical motion recorded by the long-period instrument at LASA site E1 from three large NTS explosions. All the events are displayed at identical gains; however, the gain in each case is reduced by 16 where indicated.

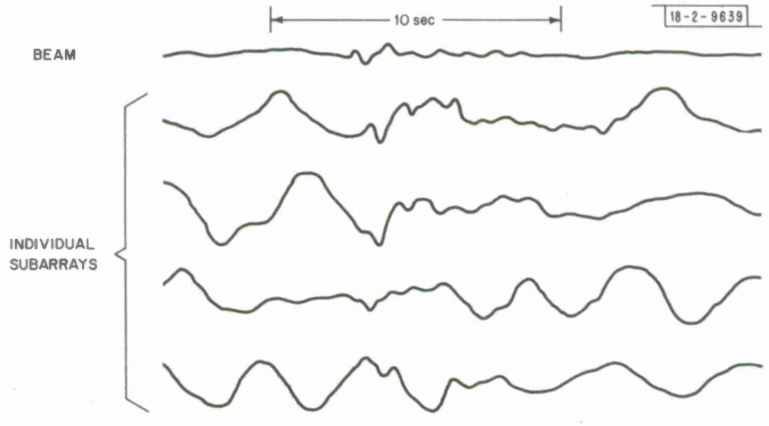

Fig. I-3. Individual LASA channels and the best beam for PKiKP from Benham.

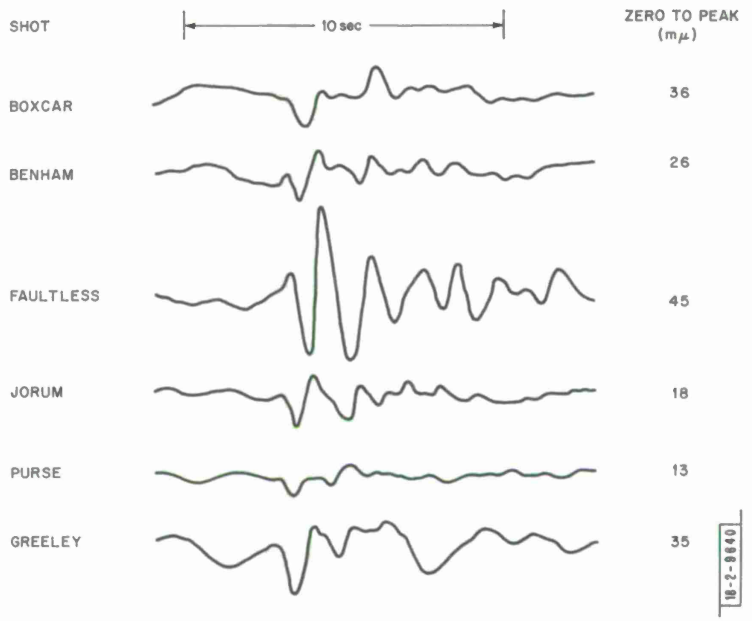

Fig. I-4. LASA beams for PKiKP from Nevada explosions.

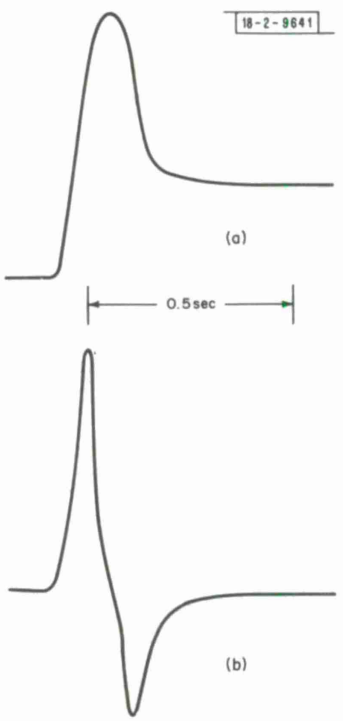

Fig. I-5(a-b). Reduced displacement potential for a 5 kt explosion in alluvium and the time derivative, which is proportional to teleseismic ground displacement (from Ref. 10).

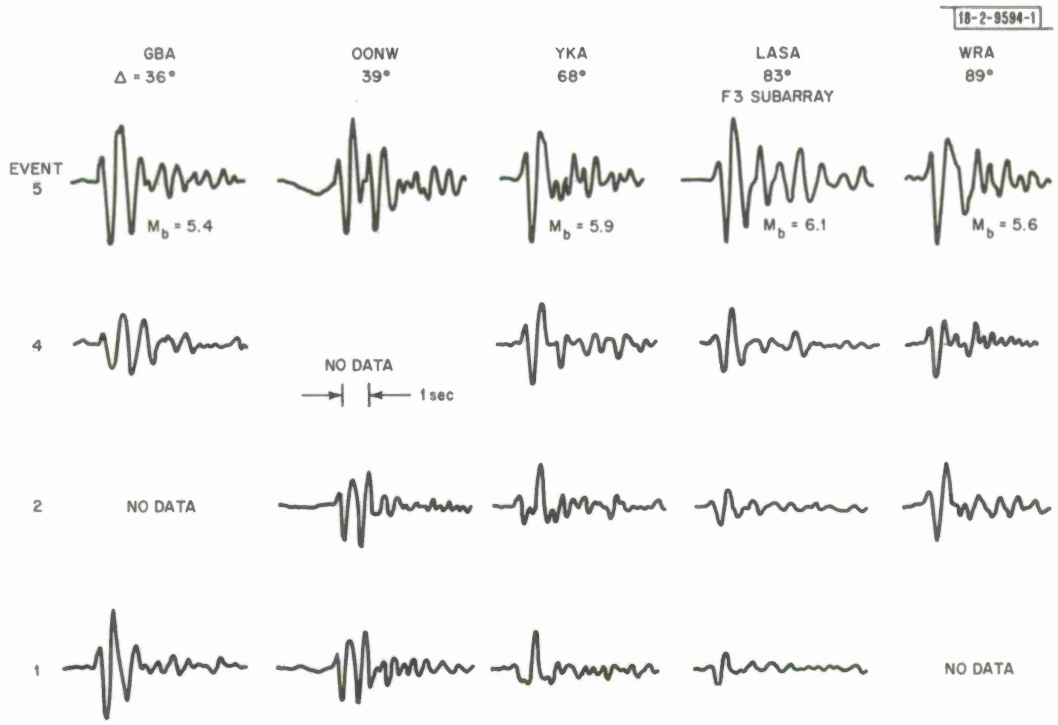

Fig. I-6. Steered beams of the P-waves from four presumed explosions in Eastern Kazakh. At each array the relative amplitudes of the events are preserved.

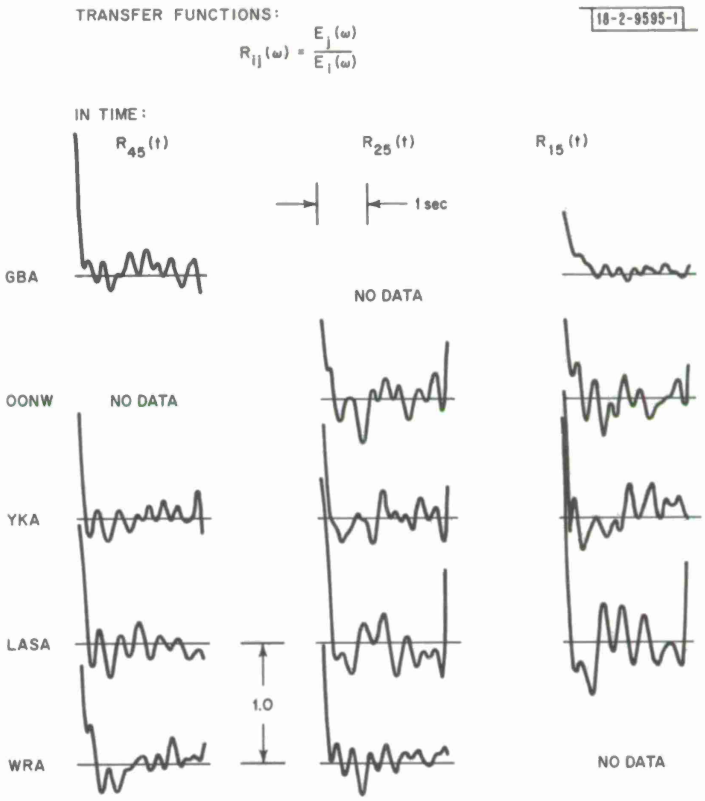

Fig. I-7. Transfer functions $R_{i5}(t)$ to shape event i to event 5 at each array.

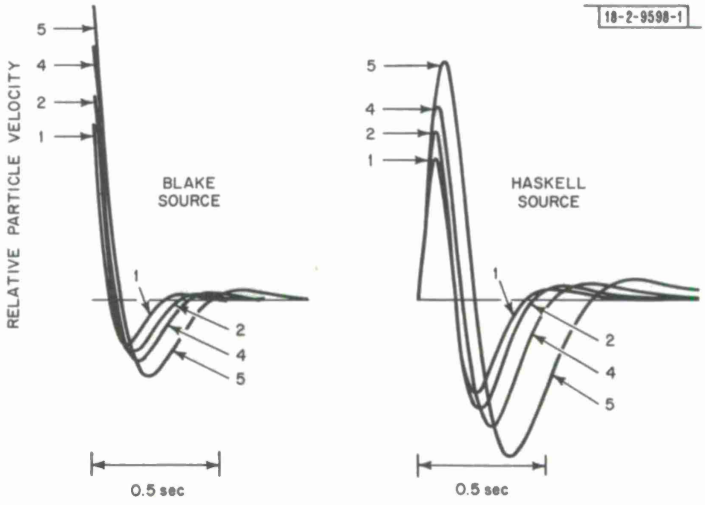

Fig. I-8. Particle velocity source functions assumed for the four events. Explosive source models of Haskell and Blake are used.

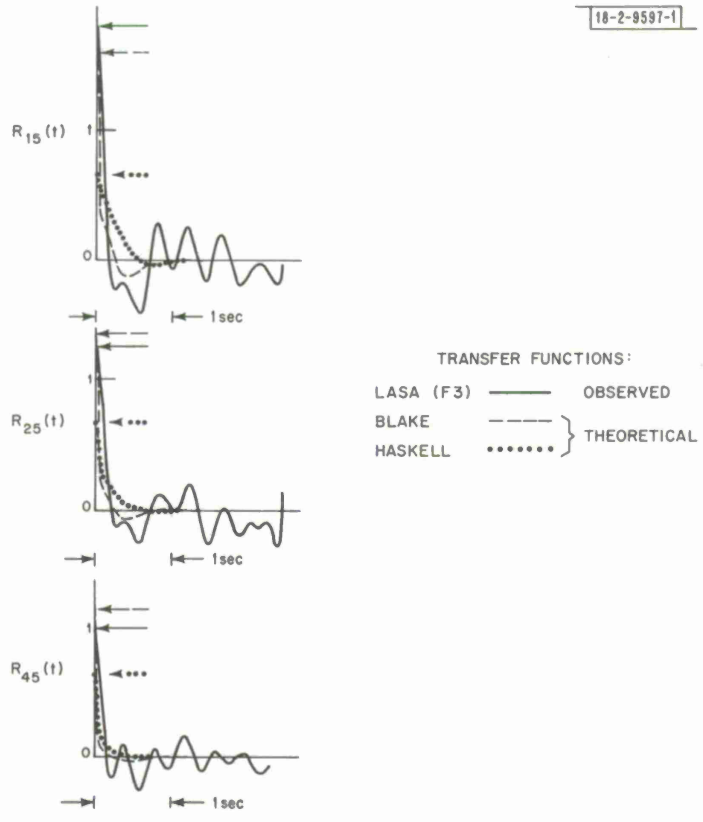

Fig. I-9. Theoretical and observed transfer functions.

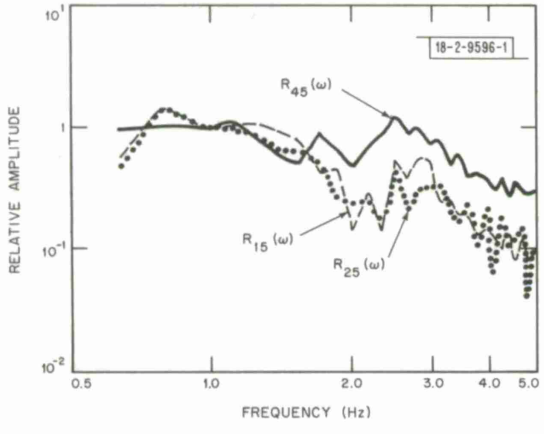

Fig. I-10. Amplitude response of observed transfer functions at LASA (F3). Plots are normalized to unit amplitude at 1 Hz.

II. PROPAGATION PATH

A. MULTIPATH PROPAGATION OF RAYLEIGH WAVES OF 40 SEC PERIOD

It is shown in Section III of this report that it is the power level of a multipath Rayleigh wave group, or any such extraneous phase, in the coda of the prefiltered Rayleigh wave train which limits the performance of the detection method which has been proposed for detecting a Rayleigh wave in the presence of the coda of a larger Rayleigh wave. Thus, it is extremely important to determine the components, as well as their power levels, which comprise the coda. Toward this end, the high-resolution wavenumber analysis method[1] was used to analyze the 40 sec period group of the prefiltered Rayleigh wave trains for ten events whose epicenters were distributed at various azimuths and distances from LASA. Measurements were made for the deviation of the azimuth of arrival from the true azimuth, in degrees, of the 40 sec period Rayleigh wave groups, during each of eight successive 200 sec intervals of time, starting with the onset time of the main 40 sec period group of the Rayleigh wave. In all cases this onset time was in agreement with the known origin time of the event and the propagation time computed from the group velocity and distance appropriate to the propagation path for the 40 sec period group.

It is interesting to compare the present results with the corresponding data for shorter periods given by Capon.[2] There is substantial agreement in the two sets of data for the angle of arrival of the main 40 sec period group. However, in the present work there are many 40 sec period multipath Rayleigh wave groups which have been detected, but were not detected previously. These multipath groups which have been detected have a power level which is quite small, relative to that of the main group. Thus, the reason these groups were not detected previously is that they were obscured by shorter-period Rayleigh wave groups which had a relatively larger power level. Hence, the prefiltering operation is essential in the present work for detecting these low power level multipath groups. However, the prefiltering operation was not essential to the study of Ref. 2, since only the major energy components of the Rayleigh wave were of interest.

The method used to obtain the propagation paths is similar to that previously employed. Two examples of such propagation paths, which were similar to or typical of the results for the rest of the ten events analyzed, are shown in Figs. II-1 and II-2. The timing sequence for the group arrivals is not shown in these figures, for simplicity. All propagation paths are drawn as straight line segments, again for simplicity. In addition, all reflections are depicted as taking place at the geographic boundaries of the continents, although they are more likely to take place at the continental margins. The difference in positions of these two boundaries is, in most cases, small and may be neglected. Only one reflection is taken into account on each epicenter-to-LASA path.

There are three propagation paths shown in Fig. II-1 for a near coast of Nicaragua event along which multipath propagation of 40 sec period Rayleigh wave groups appears to have occurred. This example was one of the most interesting of the ten events analyzed. Another interesting example is provided by the results in Fig. II-2. In this figure we see a propagation path which may be caused by a reflection at the continental margin, located in the northwestern part of North America. The propagation path for the Rayleigh wave, known as R2, which travels

around the earth in a direction opposite to that taken by the direct Rayleigh wave, known as R1, is also shown in Fig. II-2. The identification of the phase R2 was based upon wavenumber spectra measurements.

It is possible that the multipath propagation may be a consequence of scattering from diffracting objects, such as small-scale tectonic features whose dimensions are about the same as those of the wavelength of the 40 sec period group, namely 160 km (Fig. II-1 shows an apparent reflection from the Caribbean island arc).

J. Capon

B. IDENTIFICATION OF BODY-WAVE PHASES IN THE CODA OF RAYLEIGH WAVES

The wavenumber analysis of the coda of Rayleigh waves at 0.025 Hz has revealed that it is also comprised of body-wave phases, as well as surface-wave phases. The identification of these body-waves is considered below.

The wavenumber spectra for a 19 January 1968 Solomon Islands event are shown in Fig. II-3(a-c) and were obtained from prefiltered data. These wavenumber spectra indicate that there are waves propagating across LASA from the back azimuth of 87.4° with a phase velocity of about 7 km/sec. The time periods covered in Fig. II-3(a-c), relative to the origin time, are 85:22 to 88:42, 88:42 to 92:02, and 92:02 to 95:22. The travel times and horizontal phase velocities of various multiple reflected P- and S-wave phases, which propagate in the back azimuth, may be obtained from seismological tables. The phase (PS)5 is, for example, PSPSPSPSPS, with a similar notation for other phases. If we compare the data in Fig. II-3(a-c) with the travel times and velocities given in seismological tables, we see that it is possible that S6 to S8, (PS)6 to (PS)8, and (SP)6 to (SP)8 (among others) have been detected. In order to see which phases it is feasible to detect, the reflection coefficients must be examined for the given angles of incidence. The phases S6 to S8 can be ruled out, since the angle of incidence for them is between 27° to 30°, as can be obtained from Appendix V, pp. 664-666 of Ref. 3, and the reflection coefficient, at these angles, for SV-SV conversion at a free surface is very small.[4]

If we consider phases such as (PS)6, it is seen that the angle of incidence for the S-wave is still about 30°, since the major part of the path for (PS)6 is traveled as an S-wave. At this angle the reflection coefficient is near unity for SV-P conversion at a free surface. By reciprocity the reflection coefficient for P-P conversion with the same horizontal phase velocity at a free surface is near zero, and for P-SV conversion at a free surface is near unity. Thus the reflection coefficients are such that the only feasible sequences of phases are those in which P is followed by S and S is followed by P. Hence, it is possible that we have detected the phases (PS)6 to (PS)8 and (SP)6 to (SP)8. In addition, there are many other phases which are also possible, such as S(PS)6 and (PS)6P. This large number of possible phases, with the corresponding large range of arrival times, tends to explain the rather large extent in a time of ten minutes covered by the waveforms detected by the wavenumber spectra in Fig. II-3(a-c).

A similar analysis has been employed to identify other body-wave phases which comprise the coda. These phases were identified, in most cases, on the basis of phase velocity, direction of arrival, arrival time, as well as other criteria, such as reflection coefficients. The following body-wave phases have been identified among the coda of Rayleigh waves at 0.025 Hz:

(1) Multiple reflected P-waves, such as P4 and P5, which can arrive from either the front or back azimuth, and which propagate primarily in the upper mantle.

(2) Multiple reflected P- and S-waves, such as (PS)6 to (PS)8, which can arrive from either the front or back azimuth, and which propagate primarily in the upper mantle.

(3) Multiple refracted and reflected P-waves, such as P'P', which propagate through the mantle and the core.

There may be additional body-wave components of the coda which are not listed since they were not specifically detected in the present study.

J. Capon
D. Davies

C. A CHINESE PUZZLE

On 22 September 1969, an event of m_b = 5.1 was reported from the vicinity of the Chinese atmospheric test-site at Lop Nor. This region is mildly seismic and so discrimination is most important and very relevant here. The event has some interesting aspects. It appears to be an explosion on the M_s:m_b criterion, though by default, as an event which should show measurable surface waves at LASA if an earthquake, but in fact, does not. However there is at first sight clear evidence of a pP phase. We shall discuss this phase in some detail.

In Section III-B of the last SATS,[5] the composition of the coda of a seismogram from an event in Eastern Kazakh, presumed to be an explosion, was examined. We concluded that energy persisting for at least a minute after the initial phase was likely to be due to reflections beneath the source (see Fig. II-4), which we may call pdpP, where d is the depth of the reflector. Of course, reflectors beneath LASA itself, if sufficiently uniform over LASA's aperture, could produce identical signals when LASA is beamed at Eastern Kazakh. So it is necessary to learn what apparent reflectors persist for analyses of a variety of events in different places and what apparent reflectors are specific to certain locations. In the following, the reflectors we shall discuss have been through this screening process and are known not to be beneath LASA. A very extensive study of these reflectors has been completed and a discussion of the results from about 10 explosions is in preparation.

The Chinese event was passed through the VESPA process and revealed more coherent coda power from the same direction as P than any other comparable event analyzed. Figure II-5 shows a set of waveforms for this event from subarrays near the center of LASA, with the P-wave in register across the array. A large coherent energy burst occurs 15 sec after P, but there are further examples 25 sec after P and for a long way down the record. Figure II-6 shows the beam to the event, together with a beam to an Eastern Kazakh event. Other seismic stations have reported later pulses from this event, and our own examination of World-Wide Network records has also revealed them. However, there is no universal agreement on the time interval between P and the largest later phase. For instance, in the Uppsala bulletin for September 1969, Professor Båth reports "a very clear phase on the average 20.6 sec after P" from the Swedish network. The time discrepancy between Uppsala and LASA is in the wrong direction and much too large for pdpP-P interval variation as a function of Δ (which behaves similarly to pP-P interval variation). A similar remark with respect to size of discrepancy would apply

to associating Uppsala's observation with the second energy burst seen at 25 sec. For the moment we shall only comment that VESPA and the display of Fig. II-5 clearly indicate that the signal originates near the source, while other observations indicate that it is not globally coherent. Mr. L. C. Lande, our analyst, when asked to report on these waveforms, followed standard seismological practice and called the two most conspicuous energy bursts (after 15 and 25 sec) pP and sP.

Considerable effort has been devoted to establishing that this and other coherent energy from near the source region is indeed of pdpP character and not at-site activity. The most convincing argument is a slow migration of the peak power level on the vespagram toward larger values of $dT/d\Delta$ as time increases. This is consistent with a pdpP explanation in which the rays to LASA from these virtual sources (above the ground) intersect the earth's surface progressively closer to LASA as the elevation of the virtual source increases with time.

The phase after 15 sec, or p50pP, has an amplitude of half the P-wave amplitude. This requires at least a 0.5 reflection coefficient at a sharp discontinuity of 50 km depth. With any model which has been proposed thus far for the upper mantle, a reflection coefficient of this magnitude is out of the question unless there were thin, previously unobserved, layers of gross contrast in the upper mantle. However, Professor K. Aki has drawn attention to the effect that curvature of reflecting layers could have. Use of the well known mirror formula

$$\frac{1}{x_1} + \frac{1}{x_2} = \frac{2}{r}$$

for the position of source and image relative to a mirror of radius of curvature r indicates that in a very simple minded and crude way any teleseismic focussing after reflection requires concave radii of curvature of approximately twice the distance by seismic ray from the event to the reflector. For instance, a p50pP strongly insonifying LASA could imply a concave (to the source) radius of curvature of about 100 km superimposed on the deep reflector or one of double that figure at the earth's surface. Since LASA projects back to a very small area of insonified reflector beneath China (at most a kilometer in diameter), local roughnesses of reflectors of a vertical scale of the order of meters are adequate to give these concavities. Of course, such roughnesses will equally lead to defocussing and, dependent on the position of the observer, the virtual source pdpP may be either bright or dark. This "twinkling" would lead to observations such as the difference between Swedish and LASA coda structure.

Per se the subject is interesting, but it also has major repercussions on the discrimination problem. Later phases which an analyst may pick as pP, or which may add to the apparent complexity of the signal, can lead to mis-identification of an event. Furthermore, the conversion of P into pdpP en route lowers the apparent body-wave magnitude without affecting M_s, so the event moves nearer to the earthquake population. The remedy to the problem of falsely identifying pP is relatively simple, in that there must be a stringent requirement that the phase be globally observed and have concordant pP-P intervals everywhere. Some requirement that

the amplitude should not vary excessively may also be necessary. On the whole it seems desirable to err on the side of caution in using pP to call events earthquakes. Some understanding of the tectonic environment of an event is also desirable, as we have found that Eastern Kazakh events show later phases much less markedly than do presumed explosions in regions where there is higher seismicity. This subject is being pursued.

D. P-WAVE MULTIPATHING

We show in Fig. II-6 an example of what we believe to be evidence for multiple paths from source to receiver at relatively large epicentral distances ($\Delta \sim 45°$). The seismograms of the outer ring of LASA are displayed for P and PcP from an event in the Andreanof Islands (m_b = 5.2, 51.9°N, 179.1°W, h = 89 km by the USCGS). Previous work by Davies and McKenzie[6] on travel-time residuals had indicated that LASA should at least partially "see" events in this region through the sub-Aleutian plate. This plate, or region of lateral heterogeneity, will undoubtedly deform the P-wave and can lead to multiple arrivals, either by internal reflections or by refractions (see Section II-F in this report). The phase PcP should spend little time in the plate and thus be relatively simple. It is clear from Fig. II-6 that this is the case and in particular the precursor to P which is missing on PcP must be attributed to propagation path. Travel time and location studies will, of course, depend quite strongly on which signal is picked as P.

In order to show that the precursors can not be attributed to triplication in the travel time curve, we show, in Fig. II-7, a nearby earthquake (m_b = 5.5, 52.1°N, 179.9°W, h = 155 km) for which there are no precursors. Since the bulk of the propagation path is identical, we are forced to conclude that it is structure relatively near source which produces the phenomenon.

D. Davies
C. W. Frasier

E. A DIRECT MEASUREMENT OF THE EARTH'S SHORT PERIOD ATTENUATION

Measurements of the attenuation of seismic body waves within the earth are difficult because the source spectrum is rarely known. Either this spectrum must be assumed, or an assumption must be made about the effects on the spectrum of a reflection at some boundary; or one is reduced to making relative statements about attenuation along one path with respect to that along another. Measurements of ground motion taken near large underground nuclear explosions ($\Delta < 20$ km), when compared with teleseismic recordings ($\Delta > 30°$) of the same event, now allow us to measure directly the effects of the earth's attenuation.

The experiment is described diagrammatically in Fig. II-8. The assertion is that from measurements near the source, the source spectrum, S(f), is known in a given frequency band. The teleseismic spectrum, T(f), is observed in the same band and any gross difference in the shape of S(f) and T(f) is attributed to attenuation of the form $e^{-\pi t^* f}$ along the teleseismic path. Here

$$t^* = \int_{ray} \frac{ds}{Q(s)v(s)} = \frac{\tau}{Q_E} \tag{1}$$

where ds is a ray element, Q(s) is the quality parameter at s, v(s) is the compressional wave velocity at s, τ is the P-wave travel time and Q_E is the effective quality parameter. In order to measure t*, the difference

$$\delta(f) = S(f) - T(f) \tag{2}$$

is measured at specified frequencies and is considered to be of the form

$$\delta(f) = \alpha + \xi \pi f t^* \tag{3}$$

where α is a constant term encompassing geometrical spreading and instrument response and $\xi = \log_{10} e$. Then α and t* (assumed constant over the frequency band of interest) are estimated by standard least-squares procedures. The method ignores the crustal effects at the source and receiver, but our interest is in the gross differences in the spectra and not the modulation usually associated with crustal layering.

The vertical components of ground motion recorded by USCGS Carder displacement meters at three sites, 7.2, 10.8, and 11.4 km from ground zero of the Boxcar explosion, have been used to compute the source spectrum. The teleseismic spectrum has been taken from the vertical component of the P-wave recorded at the Oyer short-period subarray of NORSAR at $\Delta = 72°$. The Carder displacement meter has a flat displacement response from high frequencies up to its free period, which is usually around 2.0 sec. At frequencies lower than its free period, its response falls off as f^{-2}. The instrument is critically damped and runs with a gain of about one. The NORSAR instrument response is the same as that of LASA. Figure II-9 shows the nature of the time series data used in the experiment. The near-in trace is roughly proportional to ground displacement and the teleseismic trace to ground velocity. In the results reported here, the first two seconds, or approximately the first one and a half cycles, of near-in data were taken as representative of the far-field P radiation. By following Cagniard,[7] one can show that at 10 km the near-field term of the spherical wave solution is 0.1 that of the far-field term at 0.6 Hz and will be less at higher frequencies. At NORSAR the far-field spectrum was computed using 10 sec of the Oyer beam.

The attenuation measurements reported here were determined by a least-squares fit over the bandwidths 1.0 to 3.0 Hz and 0.6 to 3.0 Hz. Numerous experiments were conducted with varying window lengths applied to both data traces, with individual traces at NORSAR, and with various bandwidths used for fitting. In none of these experiments were the results greatly altered, nor were the standard deviations greatly changed, except when the bandwidth was extended to include frequencies as low as 0.3 Hz., This usually resulted in significantly greater attenuation values. This may be due to inaccurate determination of the damping characteristics of the near-in instruments or to contamination by the near-field term at these lower frequencies.

The results of applying the scheme described above to the data of Fig. II-9 are shown in Fig, II-10 where the frequency band 1.0 to 3.0 Hz is used. In Fig. II-10 the ordinate is in arbitrary units of displacement since it is only the shape of the spectra that is of interest. The near-in spectrum at station 465 and the NORSAR spectrum (both corrected for instrument response), the measured attenuation, and this attenuation applied to the near-in data are shown in Fig. II-10. Here the measured t* is 0.354 ± 0.038. The results using all the near-in stations and the bands 1.0 to 3.0 Hz and 0.6 to 3.0 Hz are given in Table II-1. Station 464 appears to yield a consistently lower attenuation which may be due to a local feature of that recording site.

TABLE II-1

MEASURED t* AND Q_E USING DATA FROM THREE NEAR-IN STATIONS ACROSS TWO FREQUENCY BANDS

Station	Frequency Band (Hz)	t*	Q_E		
			Low	Mean	High
463	1.0 to 3.0	0.371 ± 0.060	1590	1850	2200
464	1.0 to 3.0	0.221 ± 0.067	2370	3100	4440
465	1.0 to 3.0	0.354 ± 0.038	1750	1940	2160
463	0.6 to 3.0	0.441 ± 0.054	1380	1550	1750
464	0.6 to 3.0	0.376 ± 0.073	1520	1820	2260
465	0.6 to 3.0	0.423 ± 0.042	1470	1620	1800

These results generally support the statement of Asada and Takano[8] who, working in the same frequency band, concluded "... the value Q in the mantle cannot be as small as several hundreds." In certain mantle regions Q values may be on the order of several hundreds, but along the path from Nevada to Norway these regions must be of necessarily restricted extent. Sato[9] reviews P-wave attenuation data and reports Q values ranging from 4000 to 100 over a frequency band of 10 to 0.01 Hz. The higher Q values are associated with the higher frequency range and are consistent with the results of this experiment.

I would like to acknowledge the cooperation and assistance I have received from the U. S. Coast and Geodetic Survey Special Projects Party, Las Vegas.

J. R. Filson

F. SEISMIC RAYS IN HETEROGENEOUS MEDIA

An understanding of seismic wave propagation through realistic models of the earth is of obvious importance if information about seismic sources is to be extracted from observed data. For this reason, studies of wave propagation in three dimensional structures are currently being carried out using geometrical optics, and higher order wave propagation theories are also being investigated.

1. Ray Theory

The mathematical formulation of the ray tracing problem is given in a forthcoming Lincoln Laboratory Technical Note and will only be summarized here. If t is time and $\bar{r}(t)$ is the position vector of a disturbance on a ray, we define a slowness vector $\bar{S}$ such that

$$\dot{\bar{r}} = V^2\bar{S} \tag{1}$$

where V is the wave velocity at the point $\bar{r}$. It can then be shown that the rate of change of the slowness is

$$\dot{\bar{S}} = -\frac{\bar{\nabla} V}{V} \quad . \tag{2}$$

These two vector equations give a system of six simultaneous, first order, ordinary, differential equations which can be solved numerically to trace a ray, given its starting point and initial direction and the velocity in the earth. In practice, one of the equations can be eliminated, since the magnitude of $\bar{S}$ is $1/V$, and in cases in which the earth model has certain types of symmetry, still more equations can be eliminated. The amplitudes of the waves, considering attenuation and geometric spreading, can also be calculated, but the geometric spreading calculation involves considerable computational labor.

2. Island Arcs

Most of the current investigation has involved models of high velocity dipping slabs, such as exist in the mantle beneath island arcs, since most earthquakes occur in island arc environments. Figure II-11 shows ray paths calculated for shallow earthquakes in a simplified model of a dipping slab. The velocity outside the slab is constant, so that only effects produced by the slab appear, and the thickness, velocity contrast, and vertical extent of the slab are approximately appropriate for the Tonga arc. As the figure shows, the high velocity slab produces a large shadow, and energy is strongly focused near one edge of the shadow for earthquakes located off the axis of the slab. Clearly, these effects will have a pronounced effect on the body-wave magnitude of an event measured at a single station. The shadow produced in this manner will not be perfect; it will contain diffracted and (if the earth contains small scale heterogeneities) scattered waves. The signals observed in a shadow zone should thus be small and complex.

3. Array Location Errors

A good approximation to the error in the location calculated for an event using a seismic array such as the Montana LASA can be obtained from a ray tracing like Fig. II-11 by tracing the rays back in a straight line from the region outside the slab to the earth's surface. Errors as large as 200 km are indicated in Fig. II-11, and larger errors would occur for waves traveling closer to the direction of strike of the slab. Thus it is quite reasonable that a large part of the observed mislocation of earthquakes for LASA can be related to near source structure (see Ref. 5).

4. Travel-Time Anomalies

The observed travel-time anomalies for earthquakes of various depths in the Tonga arc have been used to try to delineate in as much detail as possible the fine structure of the slab. Waves traveling down the slab from shallow events are advanced by about 4 sec, relative to waves traveling outside the slab, while waves from earthquakes 200 km deep are advanced by only about 1.5 sec. Thus the largest velocity contrast seems to occur as the slab penetrates the low-velocity zone, at depths between about 60 and 160 km.

The magnitude of this velocity contrast is about 0.6 km/sec, or 7 to 8 percent. Even for the highly active Tonga arc, intermediate-focal-depth earthquake data are not yet numerous enough to resolve the details of the deeper parts of the slab.

5. Aleutian Arc

To compare, in as much detail as possible, the calculated and observed amplitudes, a model has been constructed for the velocity structure beneath the Aleutian arc, where the nuclear explosions Longshot and Milrow were fired. A lithospheric slab 70 km thick with a velocity of about 8.2 km/sec and a dip of 60° was assumed to extend to the bottom of the low-velocity zone. The location of the slab coincides closely with the zone of seismic activity dipping beneath the island arc. Since seismic activity stops at a depth of around 200 km, the slab was assumed to reach only to this depth. As the travel-time anomalies (see Section 4) show, the effect of a deeper part of the slab, if any exists, would be smaller than the effect of the upper part. The mantle model outside the slab is model WNA, based on $dT/d\Delta$ measurements and nuclear explosion travel times in western North America. The ray paths calculated for the Longshot explosion are shown in Fig. II-12. Energy is focused at distances around 60°, as is in fact observed (see Section II-A of Ref. 5), and amplitudes about 30 percent below normal are predicted for greater distances. The amplitudes predicted at distances less than about 60° are about normal, however, whereas the observed amplitudes are low. Some type of inhomogeneity above the slab, not included in our model, must be responsible for these observations, but its exact nature is not yet certain.

B. Julian

REFERENCES

1. J. Capon, "High-Resolution Frequency-Wavenumber Spectrum Analysis," Proc. IEEE 57, 1408-1418 (1969).
2. _____, "Analysis of Rayleigh-Wave Multipath Propagation at LASA," Bull. Seismol. Soc. Am. 60, 1701-1731 (1970).
3. C. F. Richter, Elementary Seismology (W. H. Freeman and Co., San Francisco, 1958).
4. M. Ewing, W. S. Jardetzky and F. Press, Elastic Waves in Layered Media (McGraw-Hill Book Co., New York, 1957).
5. Seismic Discrimination, Semiannual Technical Summary Report to the Advanced Research Projects Agency, Lincoln Laboratory, M.I.T. (30 June 1970), DDC AD-710613.
6. D. Davies and D. P. McKenzie, "Seismic Travel-Time Residuals and Plates," Geophys. J. 18, 51-63 (1969).
7. L. Cagniard, E. Flinn and C. Dix, Reflection and Refraction of Progressive Seismic Waves (McGraw-Hill Book Co., New York, 1962).
8. T. Asada and K. Takano, "Attenuation of Short Period P Waves in the Mantle," J. Phys. Earth 11, 25-34 (1963).
9. R. Sato, "Attenuation of Seismic Waves," J. Phys. Earth 15, 32-60 (1967).

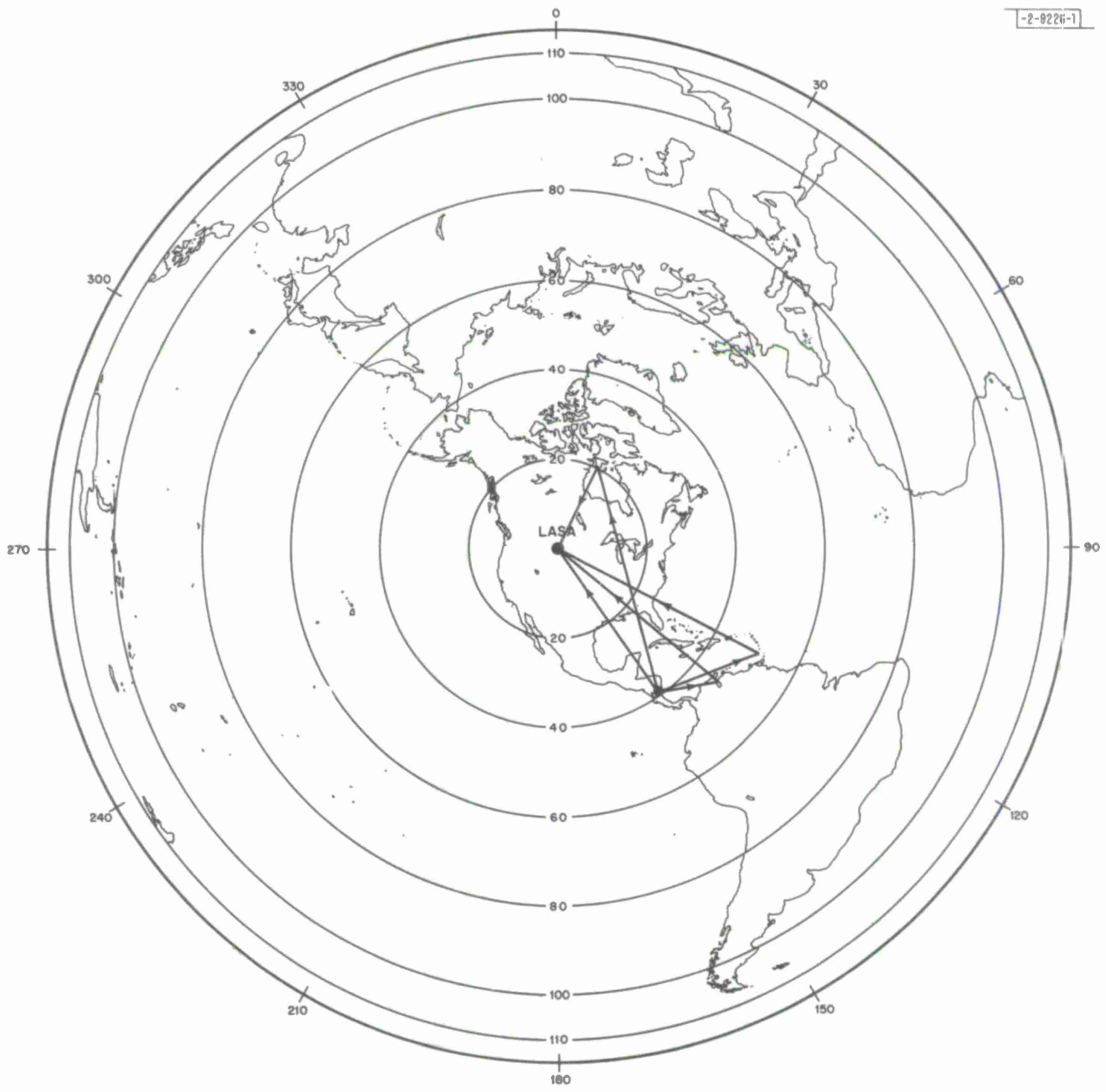

Fig. II-1. Propagation paths for the 40 sec period Rayleigh wave group for the 15 October 1967 near coast of Nicaragua event.

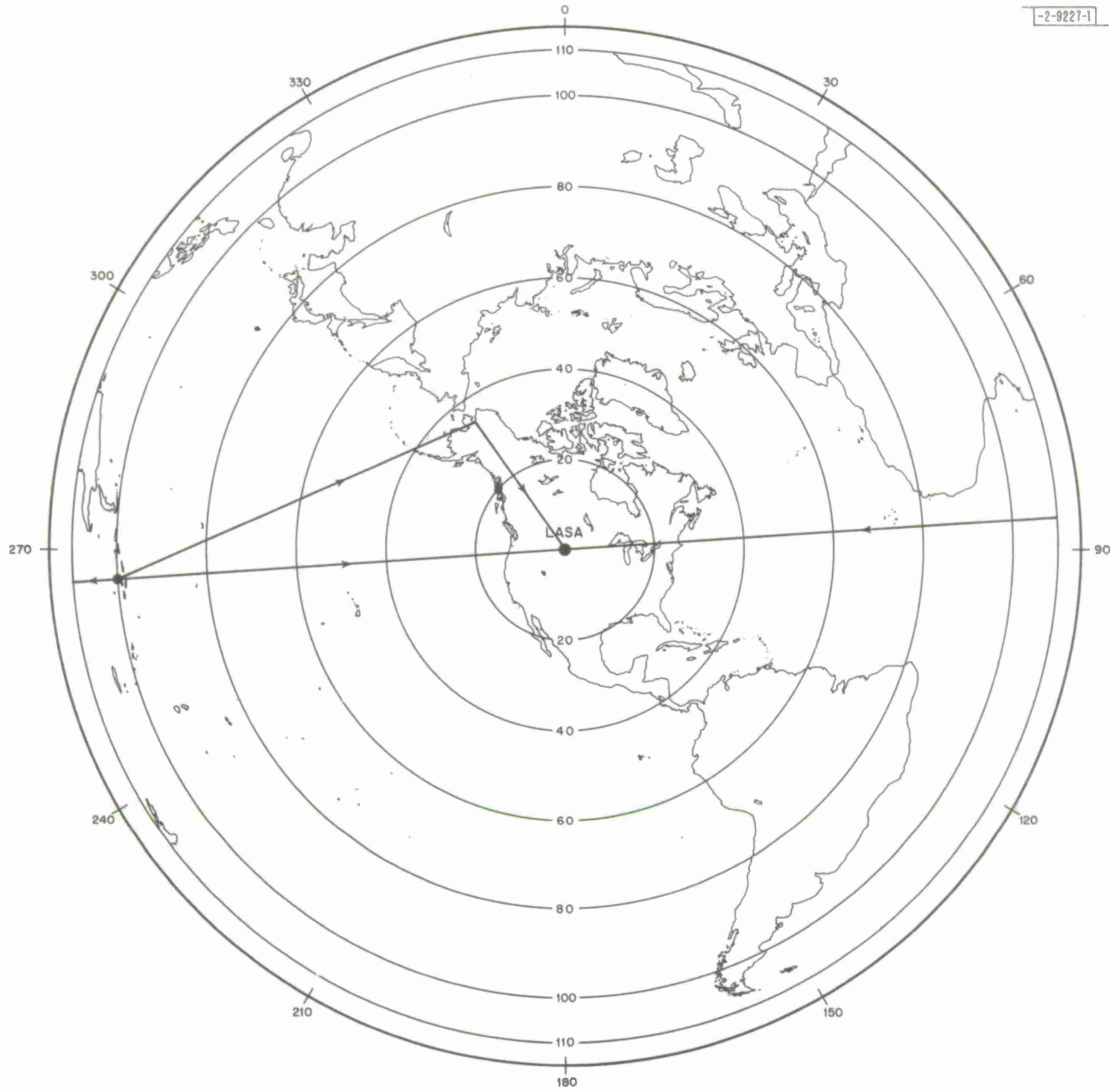

Fig. II-2. Propagation paths for the 40 sec period Rayleigh wave group for the 19 January 1968 Solomon Islands event.

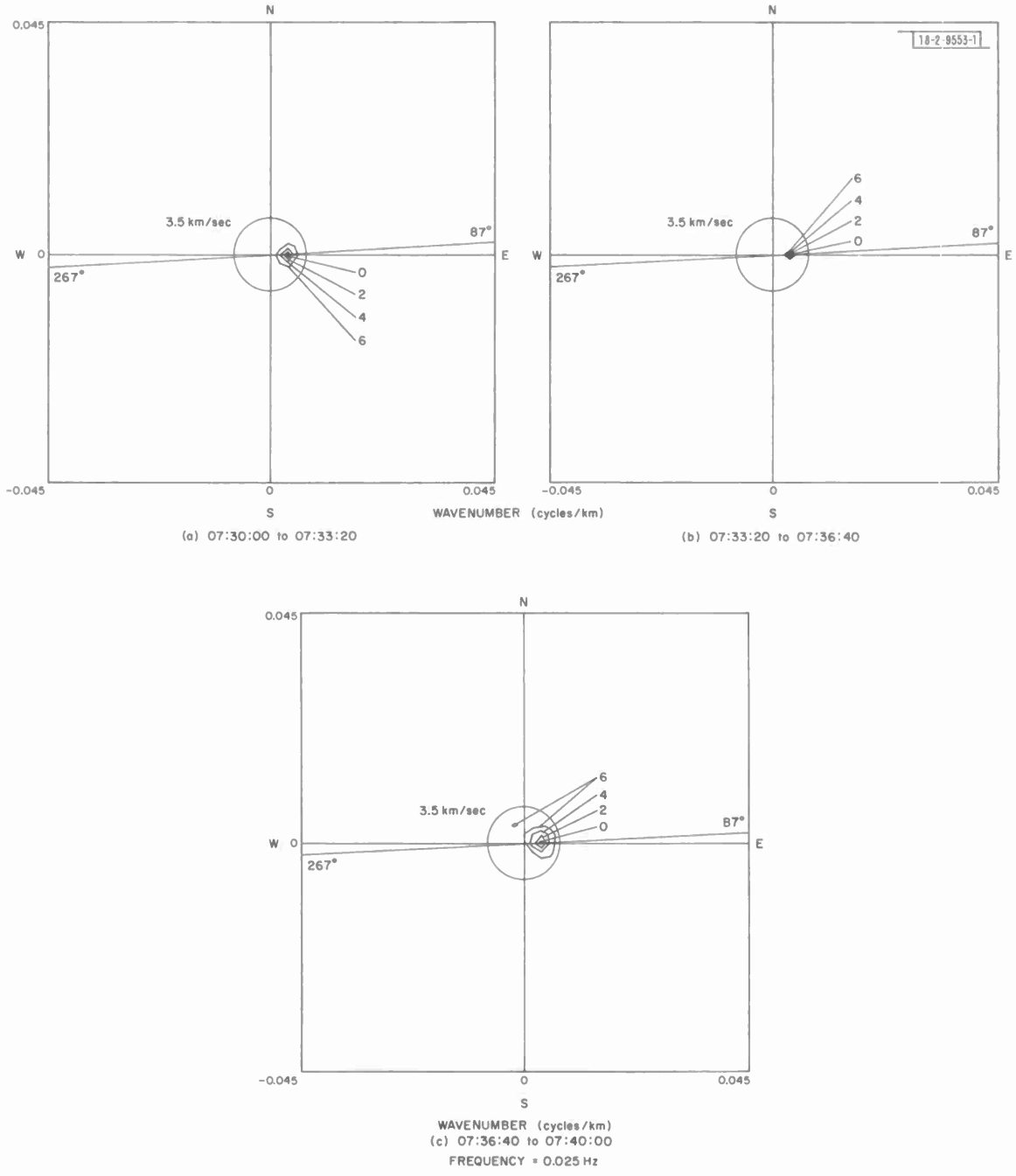

Fig. II-3(a-c). High-resolution frequency-wavenumber spectra for the prefiltered waveforms of the 19 January 1968 Solomon Islands event, illustrating the detection of multiple reflected P- and S-waves.

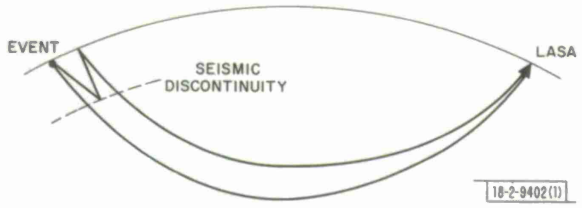

Fig. II-4. Proposed ray paths for phases in the coda.

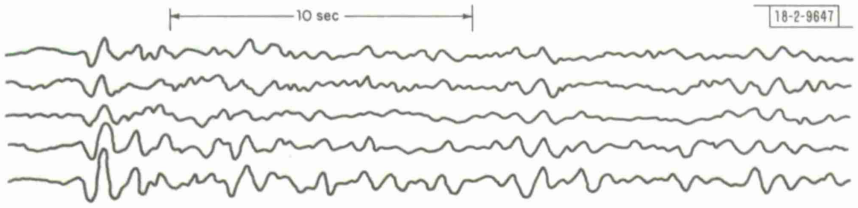

Fig. II-5. The short period seismic signals at five LASA subarrays from the Chinese event.

Fig. II-6. P and PcP from the F ring of LASA for an Andreanof Island event at 51.9°N, 179.1°W.

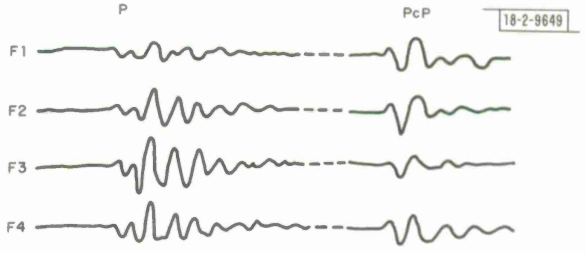

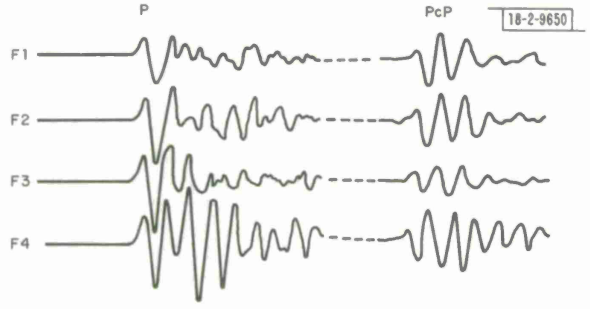

Fig. II-7. P and PcP from the F ring of LASA for an Andreanof Island event at 52.1°N, 179.9°W.

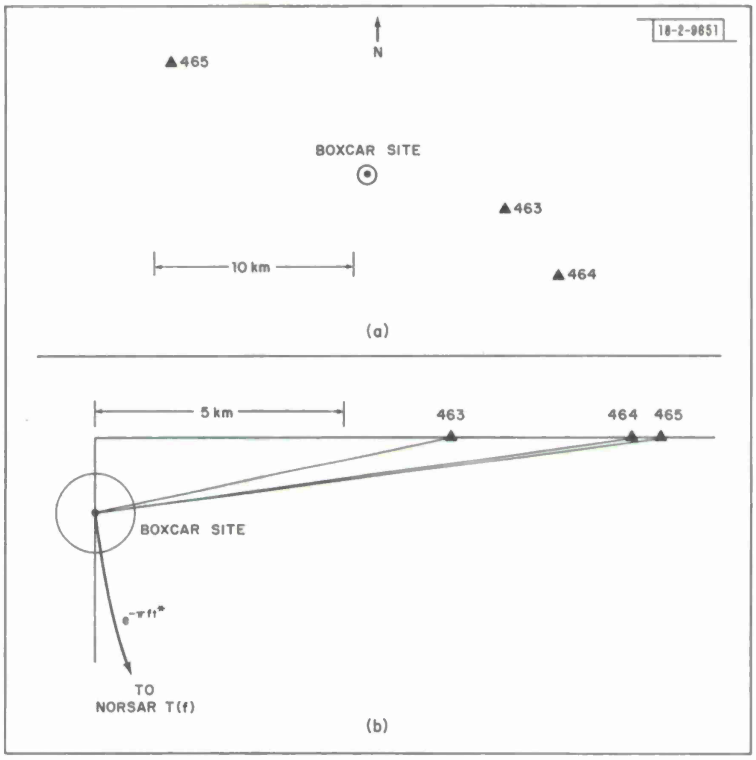

Fig. II-8. USCGS strong motion stations used relative to the Boxcar site: (a) map view; (b) composite cross section.

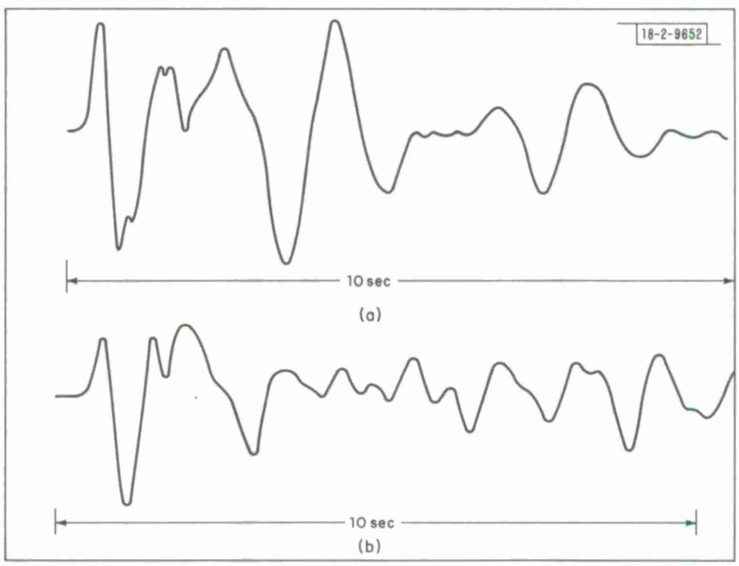

Fig. II-9. Boxcar event: (a) near-in data recorded at USCGS site 465; (b) teleseismic data recorded at NORSAR.

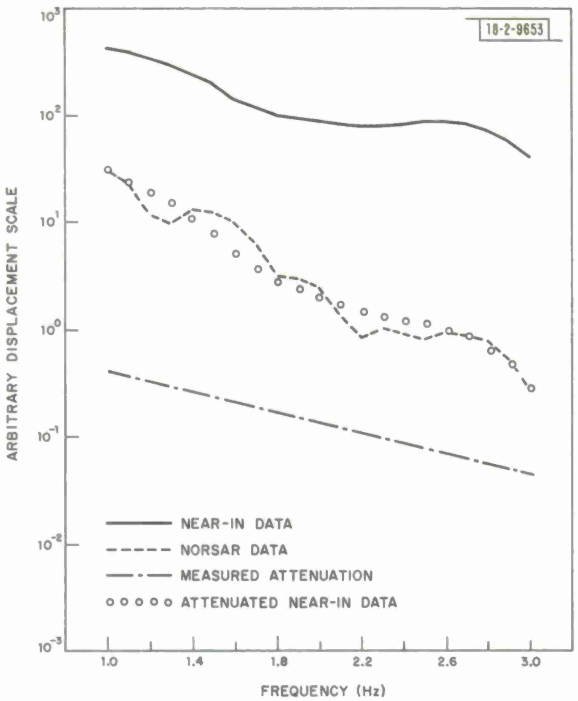

Fig. II-10. Near-in and NORSAR spectra corrected for instrument response, the measured attenuation, and the result of applying that attenuation to the near-in spectra.

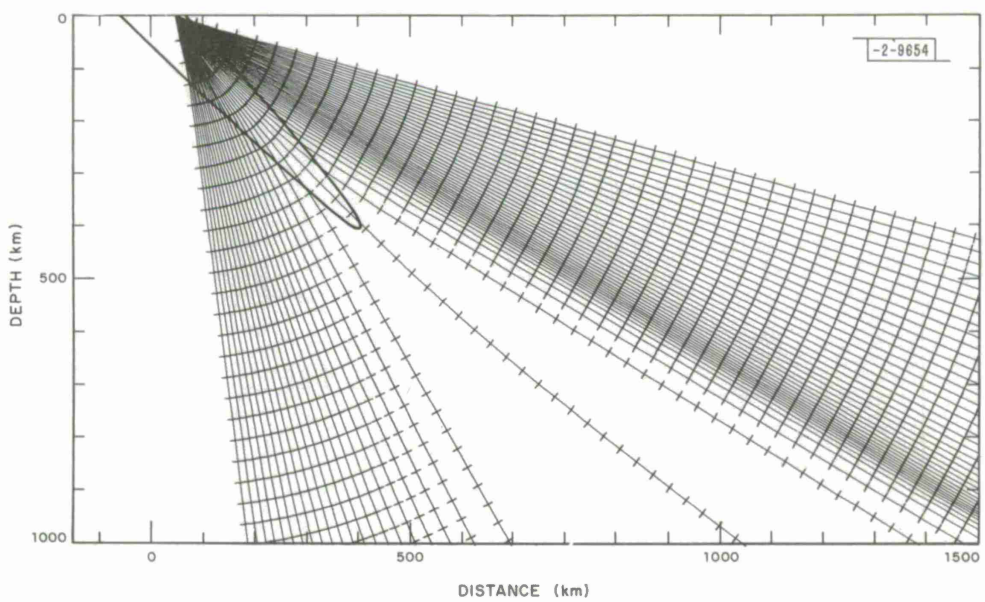

Fig. II-11. Ray paths for a source near the top edge of a simple analytic slab model. Note shadow and region of focusing of rays.

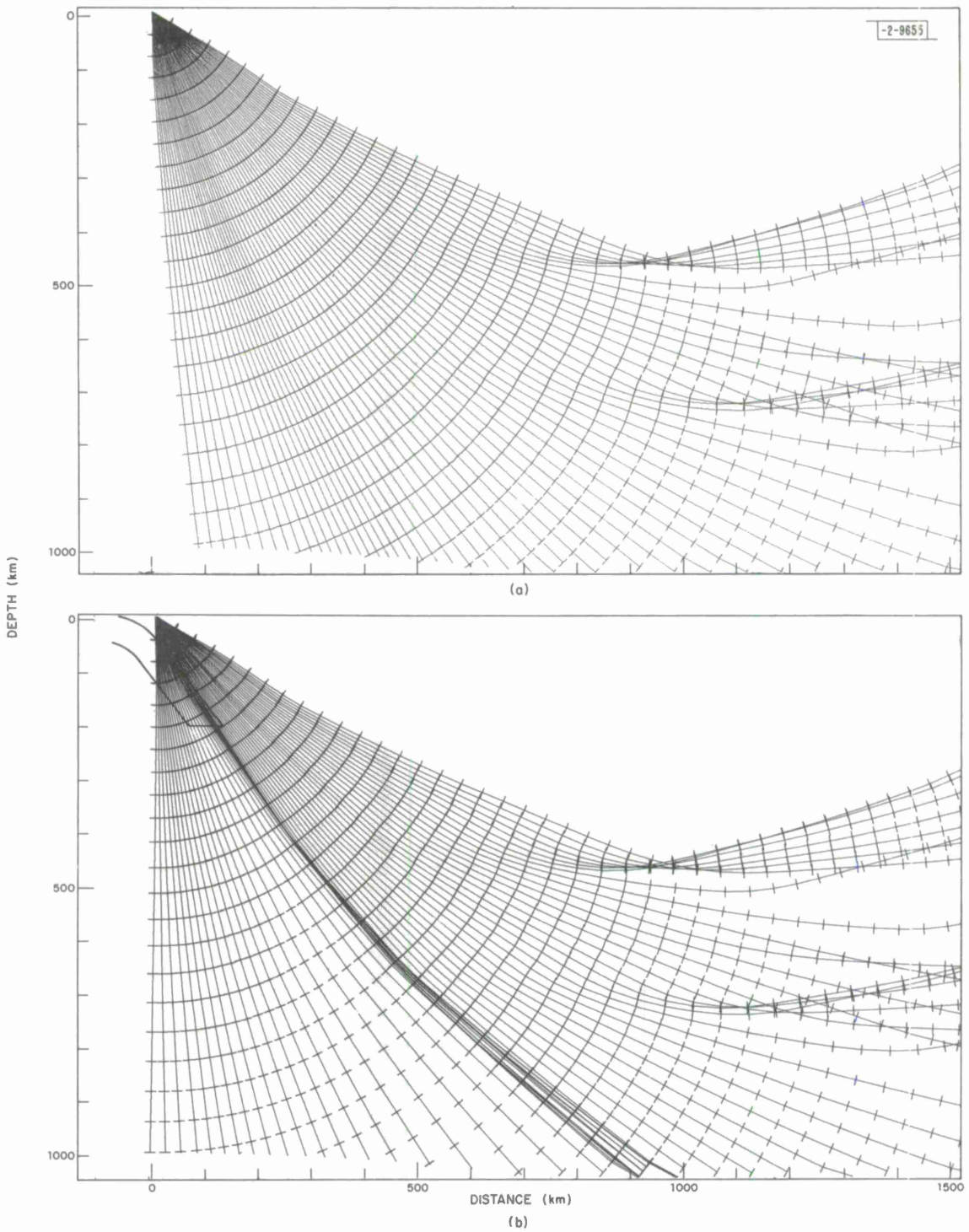

Fig. II-12. Ray paths for a realistic earth model (a) without and (b) with a slab appropriate for the Aleutian arc. The event location relative to the slab corresponds to the position of the nuclear explosion Longshot.

III. ARRAY PROCESSING

A. SOME NEW APPROACHES TO SHORT PERIOD PROCESSING FOR LARGE ARRAYS

In the past the processing of short period data from large arrays has been primarily linear. Beamforming, summing, and maximum likelihood processing are well known examples. The lack of identical waveforms at different sensors and the distortion of wavefronts have been recognized as factors which degrade array performance. Indeed, beamforming of a large array is not fruitful unless station corrections are used to straighten the wavefront. Considering the importance of signal variations for processing and discrimination the attention given this area, except for simple time anomalies, has been quite small.[1,2]

Lincoln Laboratory has now undertaken a study of these variations with several objectives in mind. First, since it is often the spectra, not waveforms, which are used for discrimination, we are investigating alternatives to beam spectra which can be used for scientific and discrimination studies. Current studies center on using the average spectra from sensors, corrected for noise bias. This has been termed spectraforming. It is possible that spectraforming will be quite important for NORSAR data, since higher frequency signals may be difficult to beamform successfully. Second, we wish to model and characterize statistically signal variations within an array and between elements in a network. This is essential to help evaluate spectraforming, to perhaps suggest other alternatives, and ultimately to evaluate discrimination capabilities. Third, the statistical properties of signal variations reflect some of the physical properties of the earth and these may be determined. Fourth, we wish to discover if new measurements of signal properties, such as spectraforming, can be used to distinguish between underground explosions and earthquakes better, especially at low magnitudes. A technical note[3] has been published detailing some of the effort thus far. Some of the ideas and results are outlined below.

Each sensor of any seismic array will contain seismic and instrumental noise as well as output generated by the signal of interest. For the present we assume the signal is sufficiently large that the background noise can be neglected. One conceptual model for signal variations is suggested by Fig. III-1. One can imagine that the signal at sensor mn is obtained from $s(t - \underline{\alpha} \cdot \underline{r}_{mn})$, which is the signal in the reference plane, by a cascade of three linear filters. The first filter is a pure time delay, τ_{mn}. The second filter is common to all sensors and represents the average change in waveform between the reference plane and the surface. The final filter represents perturbations which are specific to the particular sensor. Let $S_{mn}(f)$ be the Fourier transform of the signal at sensor mn after a time shift of $\underline{\alpha} \cdot \underline{r}_{mn} + \tau_{mn}$. We then have

$$S_{mn}(f) = S(f)T(f)\,[1 + \mathcal{H}_{mn}(f)]$$

where S(f) is the transform of s(t), T is the average waveform change, and $\mathcal{H}_{mn}(f)$ represents perturbations.

The perturbations $\mathcal{H}_{mn}(f)$ are due to fixed deterministic variations in earth structure and in that sense are not random. However, it is generally quite impossible to predict the $\mathcal{H}_{mn}$ and it is convenient to consider them to be random variables. In general, the $\mathcal{H}_{mn}$ are not independent of each other. For example, signals observed within one of the LASA subarrays are more

similar to each other than to signals drawn from other, more distant, subarrays. One way to model this phenomenon is to assume that the correlation between the H_{mn} is some decreasing function of the distance between the sensors involved. Rather than consider this general case, we have initially selected to model the situation in a way which is somewhat simpler and which uses the organization of large arrays into an array of subarrays. Specifically define

$$S_{mn}(f) = S(f)T(f)\,[1 + H_{mn}(f)]\,[1 + H_n(f)]$$

where the perturbation has been factored into two components. The factors $1 + H_n$ account for gross differences between subarrays and the $1 + H_{mn}$ for differences within the subarray. Also define

$$E[H_{mn}(f)H^*_{mn}(f)] = 2\sigma^2(f),$$

$$E[H_n(f)H^*_n(f)] = 2\sigma_A^2(f)$$

and

$$E[H_{mn}(f)H^*_{mn}(f)] = 2\sigma_S^2(f)$$

where E denotes mathematical expectation.

Let P(M,N) be average power of M sensors from each of N subarrays (a spectraform) and let $P_B(M,N)$ be the power on the beam formed from the same sensors (power from a beamform). These are both functions of frequency, but that dependence has been suppressed in the notation. Expressions for the expectation of these quantities, conditioned on S and T, have been obtained. These can be used to estimate the signal variation parameters σ_S^2, σ_A^2 and σ^2.

One way to estimate the subarray signal variation parameter σ_S^2 is to compare average power from sensors with average power from subarray beams. The ratio of expected values is given theoretically by

$$\frac{E[P(M,N)\,|\,S,T]}{E[P_B(M,1)\,|\,S,T]} = (1 + 2\sigma_S^2)\Big/\left(1 + \frac{2\sigma_S^2}{M}\right).$$

Figure III-2 shows a plot of observations of $P(M,N)/P_B(M,1)$ as measured using from 9 to 12 sensors per subarray for five subarrays in LASA. Thus, P(M,N) is the average power from about 50 sensors and the $P_B(M,1)$ used was the average power of five subarray beams. The events used were a large earthquake and a presumed underground explosion located 80° to 90° from LASA. The events are sufficiently large so that background seismic and instrument noise can be neglected.

If the H_{mn} are caused by random inhomogeneities in the earth, then the behavior of σ_S^2 as a function of frequency must depend upon the statistical properties of these inhomogeneities. We have not yet investigated this area. We have simply chosen to assume that $\sigma_S^2(f) = (C_S f)^2$. Such an assumption appears to fit the data reasonably well, but we have not yet attached any physical significance to the constant C_S. It may well be that some other function of frequency would give just as good a fit and have a better physical or theoretical basis.

Figure III-2 shows theoretical values of $E[P_B(M,N)|S,T]/E[P_B(M,1)|S,T]$ for M = 10 and several values of C_S. It appears that C_S in the range 0.3 to 0.4 gives a reasonable fit to the data. The effect of different numbers of sensors in each subarray is small and the typical number 10 has been used.

The variable $\sigma^2 = E(H_{mn}H^*_{mn})$ can be estimated using one element from each subarray of LASA. The ratio of expected average power to expected beam power is

$$\frac{E[P(1,N)|S,T]}{E[P_B(1,N)|S,T]} = \frac{1 + 2\sigma^2}{1 + \frac{2\sigma^2}{N}} \quad .$$

This is functionally the same as that for choosing instruments from within a single subarray. The ratio $P(1,N)/P_B(1,N)$ has also been calculated from the same data used for Fig. III-2. The powers, P, used were in both cases the average obtained using two different sets of 21 sensors from LASA. The data are shown in Fig. III-3. The scatter is large, but might be reduced by considering more events or using several other sets of 21 sensors. The solid curves on Fig. III-3 are given by the above equation with $\sigma^2(f) = (Cf)^2$. The value C = 1.0 appears to fit the data reasonably well, although, as noted above, the scatter is very large. It should be noted that if $(Cf)^2$ is considerably larger than unity, the signal is almost incoherent and beamforming will give almost 1/N reduction in signal power.

Another subject studied is the effect of using subarray sums from LASA rather than steering the subarrays. In the case of plane waves, the impact is well known, but has not been studied previously for partially incoherent signals. The major difference is that apparent attenuation by the subarray beam pattern is less when the signals are not identical.

In an earlier study[4] of Eastern Kazakh events it was noted that the effective path Q determined at LASA was probably too low compared to values obtained at smaller arrays. In that study beams of LASA subarray sums, and beams of individual elements of several UK arrays and of a very small Norway array were used to obtain results. Our studies of signal variations as a function of frequency can be used to help explain those results. Figure III-4 shows spectra from beams of subarray sums and average spectra at LASA. The loss of high frequencies in the beam is due, partially to the use of subarray sums, but primarily to the signal variations. The Q determination at the several sites should probably be made on the basis of average spectra, rather than beams, since the loss of high frequencies in beamforming will depend upon array size and number of sensors. If this is done, the previously determined effective Q to LASA is multiplied by roughly 1.6, the Q to the UK arrays by 1.2 and there is no change for the small Norway site. The rest of the earlier results remain essentially unchanged.

We have thus far discussed large array signal processing without much consideration of additive background noise. Unfortunately spectraforming does not reject this noise as well as does beamforming and other linear methods. This is true, even when corrections are made to remove average contributions of the noise. From this point-of-view, beamforming is a superior processing method, since it can look further down into the noise. However, it does appear that signal loss by beamforming can be sufficiently large so that spectraforming is the superior processing method for discrimination.

Figure III-5 shows average event spectra and average noise spectra for one of four events for which we have obtained such data. These data and a preliminary theoretical study have indicated that it may be possible to apply spectraforming to obtain useful spectral information for teleseismic P-waves at frequencies as large as 3.0 Hz for events in the range $4.0 \leqslant m_b \leqslant 4.5$. In general, beamforming in this range will tend to give useful information only for a small band of frequencies about the peak-power frequency of the event. Spectraforming will not be of value below 1.0 Hz and the difficulty of obtaining spectral information in that band may be the limiting factor with which we must ultimately deal.

Modifications of and additions to the Lincoln Laboratory Data Analysis Console have been undertaken to aid in the continuation of this research.

R. T. Lacoss
G. T. Kuster (M.I.T. Department of Earth and Planetary Sciences)

Seismic recordings of small seismic events observed at teleseismic distances have a high noise level relative to the signal amplitude. Although the application of an array of seismometers and different array processing techniques improve the signal-to-noise ratio considerably,[5,6,7] there still remains a residual noise whose spectrum might be significantly different from that of the signal. Consequently, further signal-to-noise enhancement should be possible through the application of noise statistics before the event's arrival. Figure III-6 shows the LASA delay-and-sum beams of three presumed explosions of different magnitudes with epicenters in Eastern Kazakh. This figure illustrates that, for the identification of small magnitude events, further noise reduction is required.

Since the energy density spectrum of a seismic signal yields a significant amount of information about the nature of the source, we have considered the energy density spectrum estimation of a seismic signal (an unknown signal) observed in the presence of an additive (short-term, stationary Gaussian[8]) seismic noise process. The conventional method of estimating the energy density spectrum of a seismic signal consists of taking the magnitude squared of the Fourier transform of the observed waveform at a single sensor or the output of an unbiased array processor. Clearly, the structure of this estimator does not depend on the noise statistics. We have defined a new estimation technique, which takes advantage of the noise statistics and yields a smaller mean square error than the conventional estimator at small signal-to-noise ratios.[9] This new estimator has a small bias but can still be useful for: (a) the estimation of the energy density spectrum of a signal recorded by an array of seismometers, and (b) the estimation of the total energy of a signal in a frequency band. Figure III-7 shows the square root of the mean square error of the conventional and new estimators of energy at a single frequency, normalized by the actual value of signal energy at that frequency, when power spectra from 100 channels, with independent additive noise processes, are averaged to obtain a final estimate. This figure illustrates that, through the application of this new estimator, a signal-to-noise ratio gain of 3 to 9 dB over that of the conventional spectraform may be obtained.

Studies of the mean and the mean square error of the spectral ratio[10] and log-likelihood ratio[11] seismic discriminants for the conventional and the new energy estimators have shown the log-likelihood ratio to be far superior in reflecting the variations in the energy estimates in the two frequency bands (Chapter III of Ref. 9) and thus should be preferred for discrimination.

Finally, a new single channel estimator of a seismic signal (an unknown transient time function) observed in the presence of an additive (short-term, stationary Gaussian) noise process is introduced and its bias and mean square error are studied (Chapter IV of Ref. 9). In defining this new estimator, we have used the new energy density spectrum estimator. Comparison of the bias and the mean square error of this new signal estimator with those of the maximum liklihood estimator (which is simply the observed waveform) shows that the new estimator, at the expense of introducing a small bias at small signal-to-noise ratios, reduces the mean square error significantly. Since some seismic discriminants are based directly on the seismic time function, one should be able to improve the identification capabilities of these discriminants through the application of this new signal estimator.

M. Mohajeri
(M.I.T., Department of
Electrical Engineering)

B. DETECTION OF INTERFERING RAYLEIGH WAVES AT LASA

The time duration of the fundamental-mode Rayleigh wave train, which initially arrives at a station and is dispersed between about 20 to 40 sec periods, is about 200 to 800 sec. This time duration is, of course, determined primarily by the distance from the epicenter to the station, and by the group velocities along the propagation path. The part of the wave train which arrives after this initial wave is called the coda and it can often persist, at significant energy levels, for a time in excess of about 5000 sec. Thus, the total time interval covered by the wave train is very large. Hence, it is quite probable that an event, A, may occur at a time such that its fundamental-mode Rayleigh wave arrives at a sensor after that of another event, B. In this case, either the fundamental-mode Rayleigh wave, or the coda, of event B, or possibly both of these wave trains, will interfere with the fundamental-mode Rayleigh wave of event A. This is especially true if the surface-wave magnitude of event B is considerably greater than that of event A. In this case, there may be considerable difficulty in detecting the Rayleigh wave due to event A, and thus it may not be possible to apply the powerful M_s:m_b criterion to determine the source type for event A. It is this problem, of detecting the Rayleigh wave of one event in the presence of the Rayleigh wave, or possibly coda, due to a larger interfering event, which has been considered in detail.

The approach that is used in detecting a Rayleigh wave in the presence of an interfering wave train is based on the use of a long-period (LP) array of seismometers. In particular the LP array at LASA was employed. Only the long-period vertical (LPZ) instruments were considered.

It appears that in most cases it is the shorter period groups of the Rayleigh wave of the interfering event that tend to obscure the detection of the longer period group of the Rayleigh wave of the desired event. It has been found that the refractions, as well as reflections, at the continental margins are usually less severe for the 40 sec period group than for the shorter period groups.[12] This is because the velocity contrast at the continental margins decreases as the period increases. Hence, a very effective method for detecting a Rayleigh wave in the presence of an interfering wave is to prefilter the LASA data so as to pass only the 40 sec period group. Then use the LASA data, in conjunction with the high-resolution wavenumber analysis method,[13] to determine the angle of arrival, as well as the arrival time of this group. It is, of course,

assumed that the expected azimuth and arrival time are known, since the epicenter and origin time of the event are assumed to be known on the basis of, say, observations of the P-wave over a reasonably large region of the earth. If this angle of arrival agrees reasonably well with the observed azimuth of the event, say within ±10°, and if the measured arrival time agrees with the arrival time, which can be computed from the known distance and group velocities for the path, to say within ±2 minutes, then the detection of the Rayleigh wave can be assumed with very little error. This is because the refractions for the 40 sec period group are very small and therefore it should arrive at the array at an angle close to the azimuth of the event. The method of detection also provides a power level for the 40 sec period group, so that a 40 sec surface-wave magnitude of the event may be determined. This means that the M_s:m_b criterion can then be used to determine the source type of the event, assuming that the P-wave has also been detected.

A number of simulation experiments were performed, using actual seismic data, for the purpose of evaluating the capabilities, as well as the limitations, of the method which has been proposed for detecting one Rayleigh wave in the presence of the coda of another larger Rayleigh wave. One of the simulation experiments will now be described.

The waveforms for a 21 November 1966 Kurile Islands event and a 2 March 1967 Ecuador event were added together and applied to a low-pass filter, which effectively filters all groups of period less than 40 sec. The waveforms were summed in such a way that the onset time of the 40 sec period group of the Kurile Islands event, in the resultant waveform, was delayed by about 200 sec relative to that of the Ecuador event. An amplitude weight was applied to the waveforms of the Ecuador event so that the power level of its 40 sec period group was approximately the same as that of the Kurile Islands event in the resultant prefiltered summation waveform. This amplitude weight was then diminished successively three times in steps of −10 dB, for a total of −30 dB relative to the initial value of the amplitude weight. The purpose of this successive attenuation is to illustrate the operation of the detection method. The resultant prefiltered summation waveforms, for only the sensors at A0 and the F ring, are shown in Fig. III-8(a-d). The power level of the 40 sec period group of the Ecuador event is 4 dB, −6 dB −16 dB, −26 dB, relative to that of the Kurile Islands event in (a) through (d) of Fig. III-8, respectively. In addition to the main group arrival for the Kurile Islands event, there is a multipath Rayleigh wave group arrival due to this event which occurs during the time occupied by the main group arrival of the other event. This multipath group, which is barely visible in (d) of Fig. III-8, will determine the limits of the performance of the detection method. The power level of this multipath group is 13 dB below that of the main group of the Kurile Islands event and thus the power level of the main group of the Ecuador event is 17 dB, 7 dB, −3 dB, −13 dB relative to that of the multipath group of the Kurile Islands event in (a) through (d) of Fig. III-8, respectively. These various power levels are indicated in Fig. III-8(a-d). In addition, the time scales at the top and bottom of each of these figures pertain to the Kurile Islands and Ecuador events, respectively.

The results, obtained when the high-resolution wavenumber analysis (HR) method is applied to the second 200 sec of the data in Fig. III-8(a-d), are shown in Fig. III-9(a-d), respectively. In Fig. III-9(a) the direction of arrival of the main group of the Ecuador event, at the appropriate time, is indicated quite well. However, in Fig. III-9(b) and (c) the multipath group due to the Kurile Islands event is indicated as arriving at an azimuth which differs from the true azimuth of that event by about 16°, while the main group arrival of the other event is also detected.

However, in Fig. III-9(d) only the multipath group of the Kurile Islands event is detected, since its power level is large enough relative to that of the main group of the other event so as to obscure the detection of this group. Thus, we see that it is the power level of the main group relative to that of a multipath Rayleigh wave group, or any such extraneous phase, which limits the performance of the detection method. It has been found experimentally that the value of this relative power level at the threshold condition is variable, but that −6 dB is an average value.

It has been shown that the power level of the coda, as well as that of the main group, of the prefiltered Rayleigh wave train determines the detection threshold of the detection method. Thus, in order to determine this detection threshold, it is necessary to measure this power level at various times during the extent of the coda. The detection threshold, or the power level of the desired 40 sec period Rayleigh wave group at which it is still possible to determine its azimuth of arrival using the HR method, is then about 6 dB below the power level of the coda. The manner in which the power level of the coda of the prefiltered data decreases as a function of the time after the onset time of the main group, for ten events whose epicenters are distributed at various azimuths and distances from LASA, is shown in Fig. III-10(a). It is seen from this figure that the decrease of the coda power level is quite variable for the events analyzed.

The data in Fig. III-10(a) were used to determine the minimum, average and maximum detection thresholds for the detection method as a function of the difference in arrival times of the main groups, and the results are shown in Fig. III-10(b). Thus, it is seen from Fig. III-10(b) that if a 40 sec period Rayleigh wave group arrives at LASA and is followed 600 sec later by another group, then, as an average value, we can expect to detect the second group, provided its power level or amplitude is not more than 24 dB below that of the first group. However, there are some events for which the corresponding value would be only 14 dB, while there are others for which it would be a very impressive value of 40 dB.

J. Capon

C. AMPLITUDES OF P AND PcP PHASES AT LASA

Short-period P and PcP phases are being studied at LASA to see how consistent PcP/P ratios are for a given event recorded at all LASA subarrays. Examination of eight events in a narrow azimuthal sector 303° to 317° indicate that the peak-to-trough amplitude patterns of both P and PcP phases over the entire array are complex and dissimilar for epicentral distances (Δ) out to 63°. In fact, the large scatter of PcP/P ratios noted by Martner,[14] Buchbinder,[15] and Kanamori[16] at stations a degree or so apart, can be observed at LASA from subarray to subarray ($\gtrsim$10 km apart). Of great interest, however, is that the P and PcP amplitude patterns are not random, but can be duplicated by closely located events of different depths, the PcP pattern being more consistent than the P pattern with variations in epicentral distance. This indicates that differences in P and PcP amplitude patterns are caused by complex transmission and diffraction of the seismic signals by the structure under LASA, rather than by angular variations in radiation at the source. This also implies that the core-mantle boundary is locally smooth over apertures of at least the two degrees sampled by the data.

Table III-1 is a list of the events studied. Events 1 to 6 are closely spaced in the Andreanof Islands at about 45° from LASA and events 7 and 8 are off the western coast of Kamchatka at about 60° from LASA.

TABLE III-1

ALEUTIAN EVENTS STUDIED

Event	Date	Arrival Time	Latitude (deg)	Longitude (deg)	Δ (deg)	Azimuth (deg)	m_b	m_b (LASA)	Depth (km)
1	21 February 1968	06:28:53	52.3N	175.3W	43.7	303.8	5.3	5.3	107
2	22 June 1967	15:44:42	51.7N	176.8W	44.7	303.5	5.3	6.6	54
3	19 December 1967	14:48:51	51.7N	176.9W	44.8	303.6	4.8	5.5	59
4	23 February 1968	20:37:46	51.9N	179.1W	46.0	304.6	5.2	5.3	89
5	11 August 1968	12:45:33	52.1N	179.9W	46.4	305.1	5.5	5.6	159
6	29 October 1965	21:08:36	51.4N	180.8W	47.2	304.6	5.8	6.1	0
7	9 October 1967	14:20:09	54.1N	155.1E	58.3	316.8	5.2	6.0	393
8	8 January 1968	14:00:38	49.1N	151.3E	63.3	314.1	5.0	5.8	284

Events 1 to 6 are separated into two groups, shallow and deep. Figure III-11 shows the relative amplitudes of P and PcP phases measured at each subarray of LASA for the three shallowest events. Event 6 is the nuclear test Longshot fired on Amchitka Island. To show the similarity of the amplitude patterns, the P and PcP amplitudes were normalized so that the average PcP amplitude for each event is 1.

The PcP amplitude patterns are quite consistent for the three events, and no apparent difference between Longshot and the two shallow earthquakes is seen. The P amplitudes are also self consistent, except for those of Longshot, many of which were clipped.

Figure III-12 shows amplitudes for the three deepest events. Although the average level of P amplitudes for these events is significantly closer to the PcP level, the amplitude patterns across LASA are the same as those shown in Fig. III-11. Of particular interest is that the P and PcP patterns for the inner subarrays of LASA are completely out of phase in both figures. Clearly, the structure beneath these regions, distorts P and PcP unequally. This makes it very inadvisable to use individual subarrays for relative amplitude studies such as PcP/P ratios for core-mantle boundary structure.

For epicentral distances greater than 45° it has been assumed[15,16] that the signal distortion introduced by the crust under each receiver is the same for P and PcP waves. In order to test this, P and PcP amplitude patterns should merge for a large enough epicentral distance (Δ). This effect can be partially seen for events 7 and 8 plotted in Fig. III-13. The P and PcP amplitude patterns match fairly well for the F and E rings, but are still somewhat out of phase at the inner rings. This suggests that reliable PcP/P ratios can be obtained only from the individual sites of the F and E rings for $\Delta \approx 58°$ to 63° along this northwestern azimuth.

Figure III-14 shows the P and PcP phases recorded on the F ring for event 7. It can be seen that site F4 produces a ringing wave form on both P and PcP phases whereas F1 produces more impulsive phases. Thus, F1 lets through a broader band of frequencies than F4 for both P and PcP phases at this distance. This is also verified by the amplitude spectra of the individual phases as shown in Figs. III-15 and III-16.

In summary, the amplitude patterns of P and PcP phases at LASA seem to be dominated by the diffraction effects of the structure under LASA. It must be emphasized that such effects can only be detected by using array data. Until these effects are understood, it appears difficult to interpret PcP/P ratios over a wide range of epicentral distances from LASA in terms of the core-mantle boundary. This also indicates that data from isolated stations may be considerably less reliable for amplitude studies of core phases than previously supposed.

C. W. Frasier

REFERENCES

1. H. Mack, "Nature of Short-Period P-Wave Signal Variations at LASA," J. Geophys. Res. 74, 3161-3170 (June 1969).
2. J. Capon. R.J. Greenfield, R.J. Kolker and R.T. Lacoss, "Short-Period Signal Processing Results for the Large Aperture Seismic Array," Geophysics 33, 452-472 (1968), DDC AD-674830.
3. R.T. Lacoss and G.T. Kuster, "Processing a Partially Coherent Large Seismic Array for Discrimination," Technical Note 1970-30, Lincoln Laboratory, M.I.T. (27 November 1970).
4. Seismic Discrimination, Semiannual Technical Summary Report to the Advanced Research Projects Agency, Lincoln Laboratory, M.I.T. (30 June 1970), Sec. I-A, DDC AD-710613.
5. J. Capon, R.J. Greenfield and R.J. Kolker, "Multidimensional Maximum-Likelihood Processing of a Large Aperture Seismic Array," Proc. IEEE 55, 192-211 (1967), DDC AD-651722.
6. R.T. Lacoss, "Adaptive Combining of Wideband Array Data for Optimal Reception," IEEE Trans. Geosci. Electron. GE-6, 78-86 (1968), DDC AD-673599.
7. P.E. Green, Jr., E.J. Kelly, Jr. and M.J. Levin, "A Comparison of Seismic Array Processing Methods," Geophys. J.R. Astr. Soc. 11, 67-84 (1966), DDC AD-649184.
8. R.A. Haubrich, "Earth Noise, 5 to 500 Millicycles per Second," J. Geophys. Res. 70, 1415-1427 (1965).
9. M. Mohajeri, "Seismic Discrimination in the Low Magnitude Range," M.I.T., Sc. D. Thesis, December 1970.
10. R.T. Lacoss, "A Large-Population LASA Discrimination Experiment," Technical Note 1969-24, Lincoln Laboratory, M.I.T. (8 April 1969), DDC AD-687478.
11. Seismic Discrimination, Semiannual Technical Summary Report to the Advanced Research Projects Agency, Lincoln Laboratory, M.I.T. (31 December 1968), Sec. I-B, DDC AD-682297.
12. J. Capon, "Analysis of Rayleigh-Wave Multipath Propagation at LASA," Bull. Seismol. Soc. Am. 60, 1701-1731 (1970).
13. J. Capon, "High-Resolution Frequency-Wavenumber Spectrum Analysis," Proc. IEEE 57, 1408-1418 (1969).
14. S.T. Martner, "Observations on Seismic Waves Reflected at the Core Boundary of the Earth," Bull. Seismol. Soc. Am. 40, 95-109 (1950).
15. G.G.R. Buchbinder, "PcP from the Nuclear Explosion Bilby, September 13, 1963," Bull. Seismol. Soc. Am. 55, 441-461 (1965).
16. H. Kanamori, "Spectrum of P and PcP in Relation to the Mantle-Core Boundary and Attenuation in the Mantle," J. Geophys. Res. 72, 559-572 (1969).

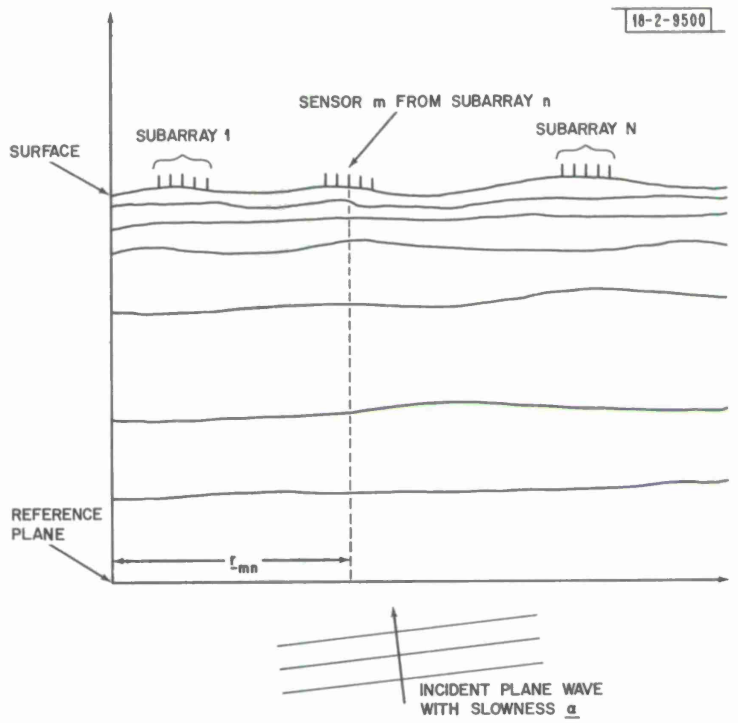

Fig. III-1. Schematic of body wave incident upon a large seismic array.

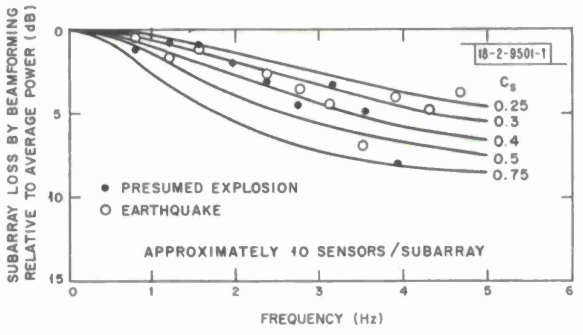

Fig. III-2. Subarray power loss by beamforming relative to a single sensor vs frequency. Theoretical curves shown for $\sigma_S^2 = C_S^2 f^2$.

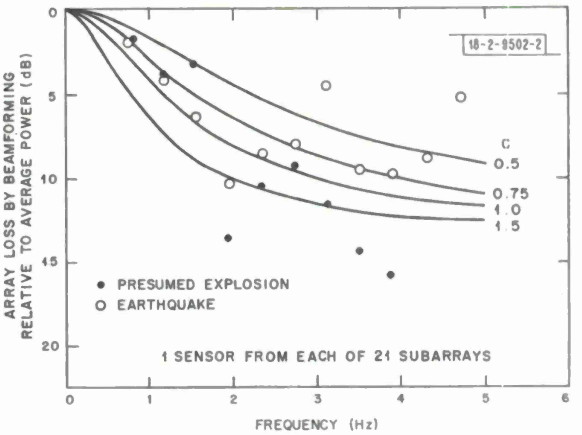

Fig. III-3. Array loss by beamforming relative to a single sensor vs frequency. Theoretical curves shown for $\sigma^2 = C^2 f^2$.

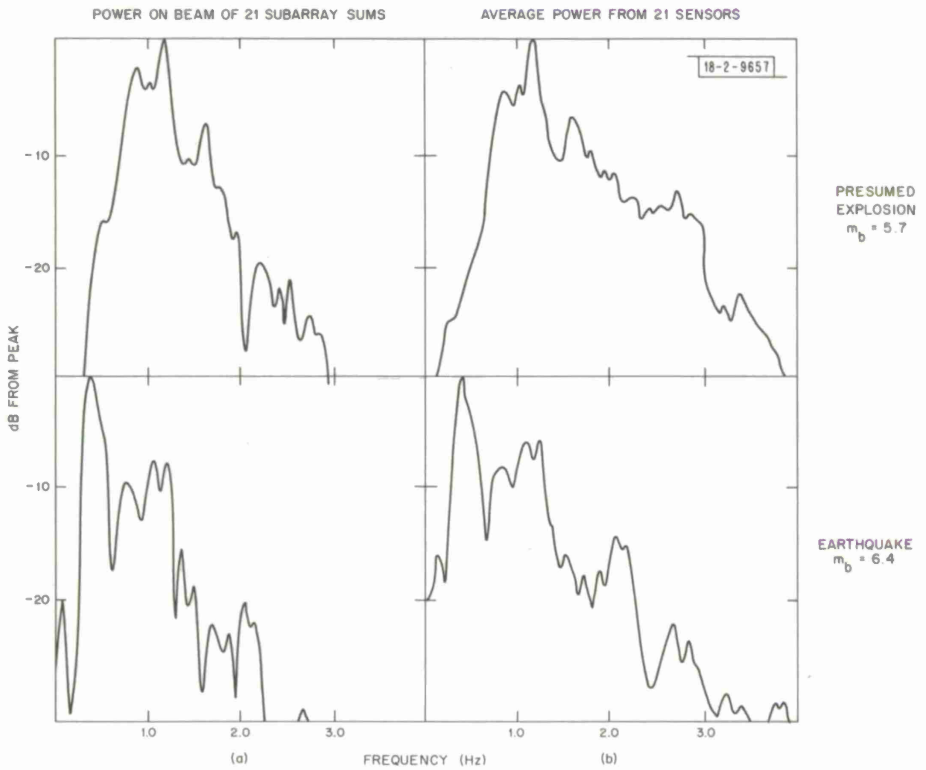

Fig. III-4. Power spectra obtained from: (a) transform of beam of subarray sums; (b) average power on individual instruments.

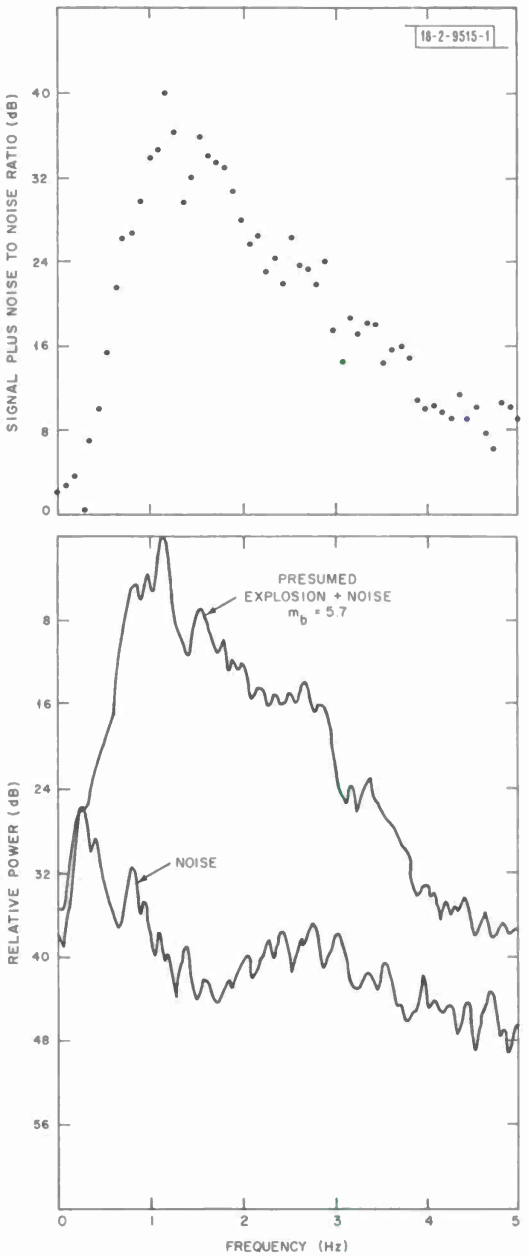

Fig. III-5. Average event power spectrum for a large event and for background noise.

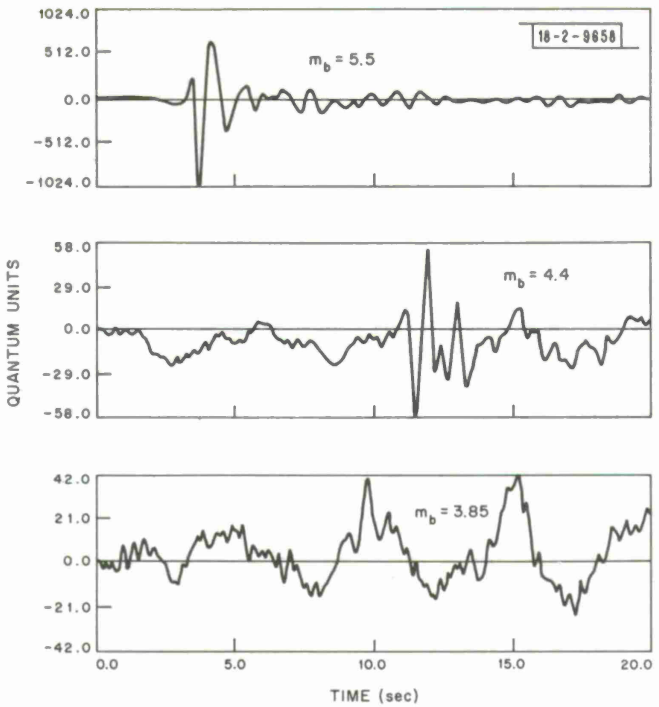

Fig. III-6. LASA delay-and-sum beams for three seismic events with different body-wave magnitude, m_b, from Eastern Kazakh. One quantum unit = 0.04 mμ at 1 Hz.

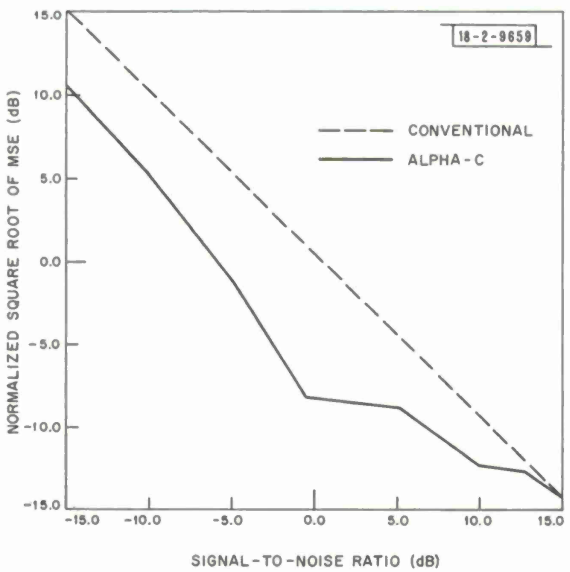

Fig. III-7. Normalized square root of the mean square error of the conventional and ALPHA-C estimators of power density using 100 channels.

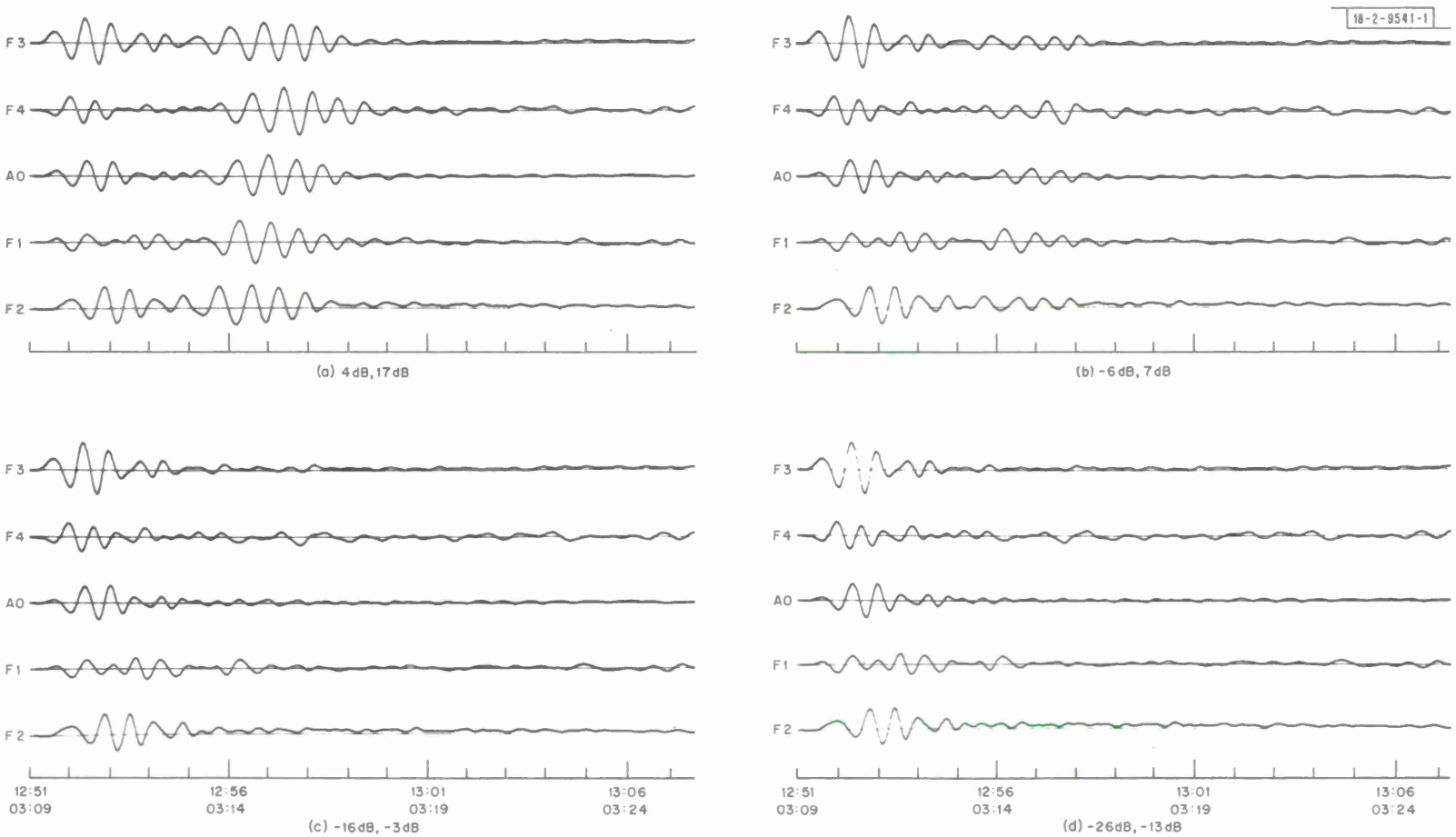

Fig. III-8(a-d). Waveforms used in simulation study.

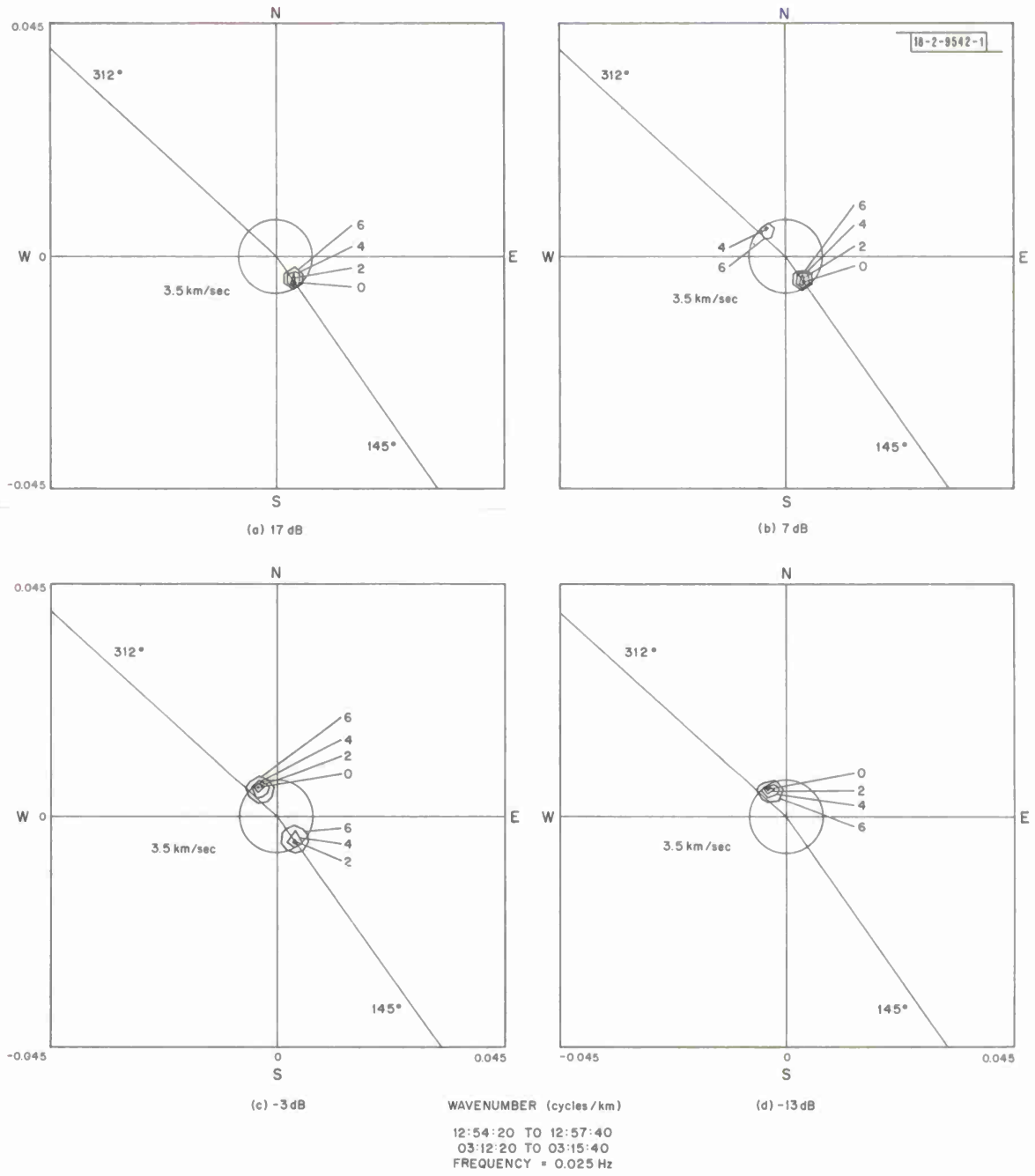

Fig. III-9(a-d). High-resolution frequency-wavenumber spectra for artificial waveforms at 0.025 Hz.

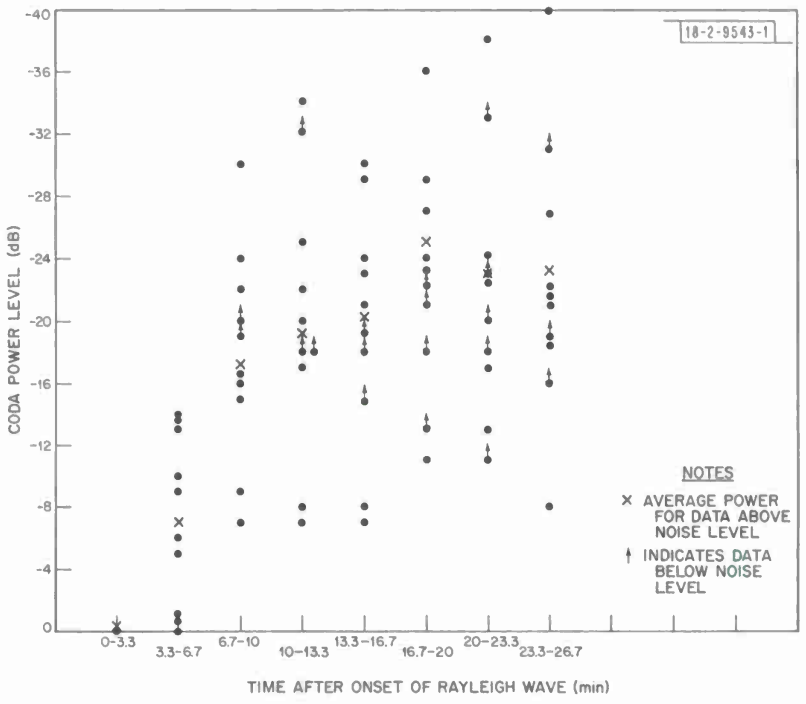

Fig. III-10(a-b) Rate of decay of coda power level and performance characteristic of proposed detection method.

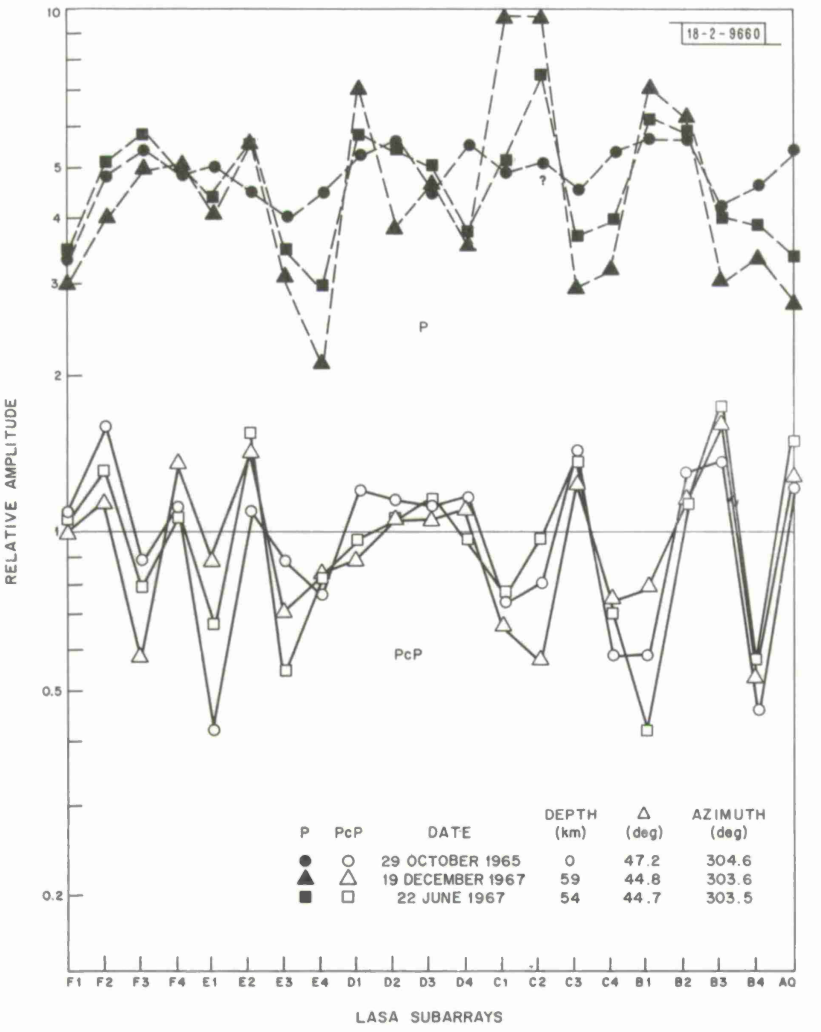

Fig. III-11. Amplitude patterns of P and PcP phases across LASA for three shallow Andreanof Island events.

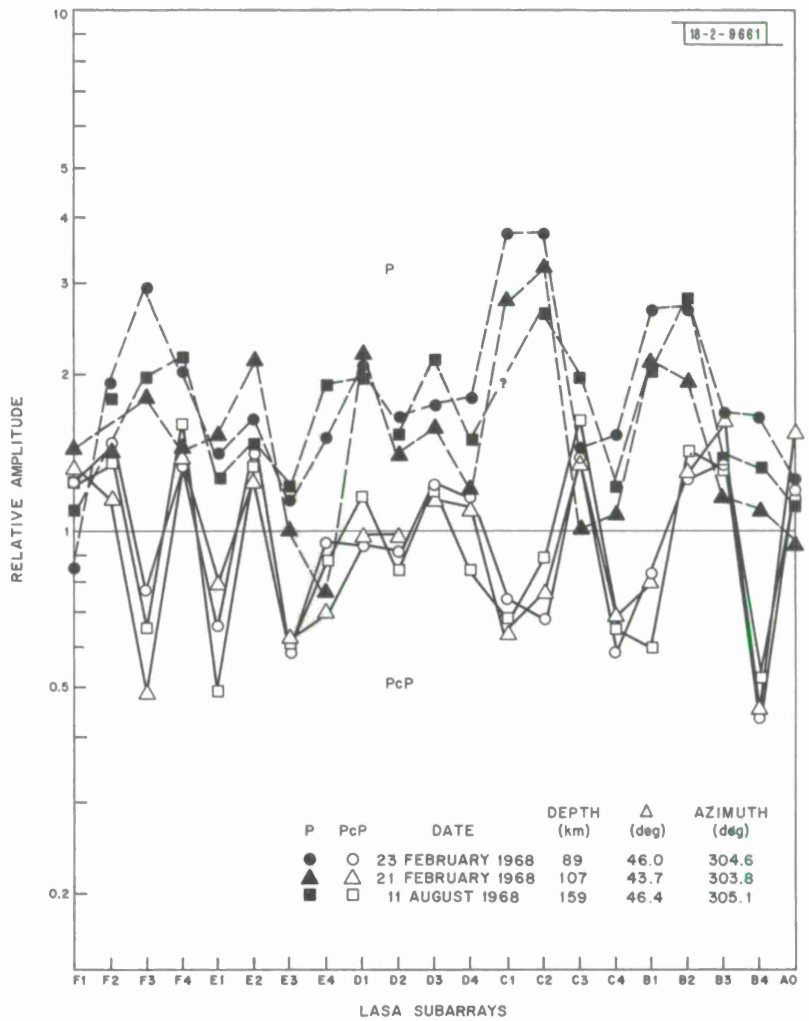

Fig. III-12. Amplitude patterns of P and PcP phases across LASA for three deep Andreanof Island events.

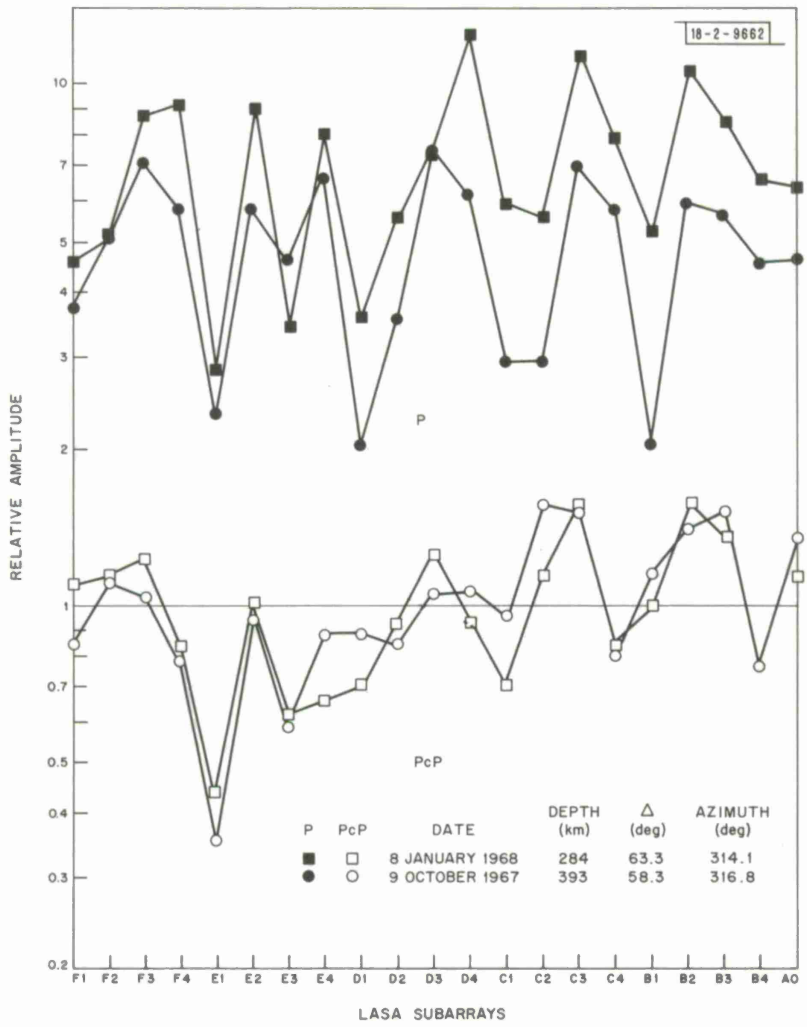

Fig. III-13. Amplitude patterns of P and PcP phases across LASA for two deep events off western coast of Kamchatka.

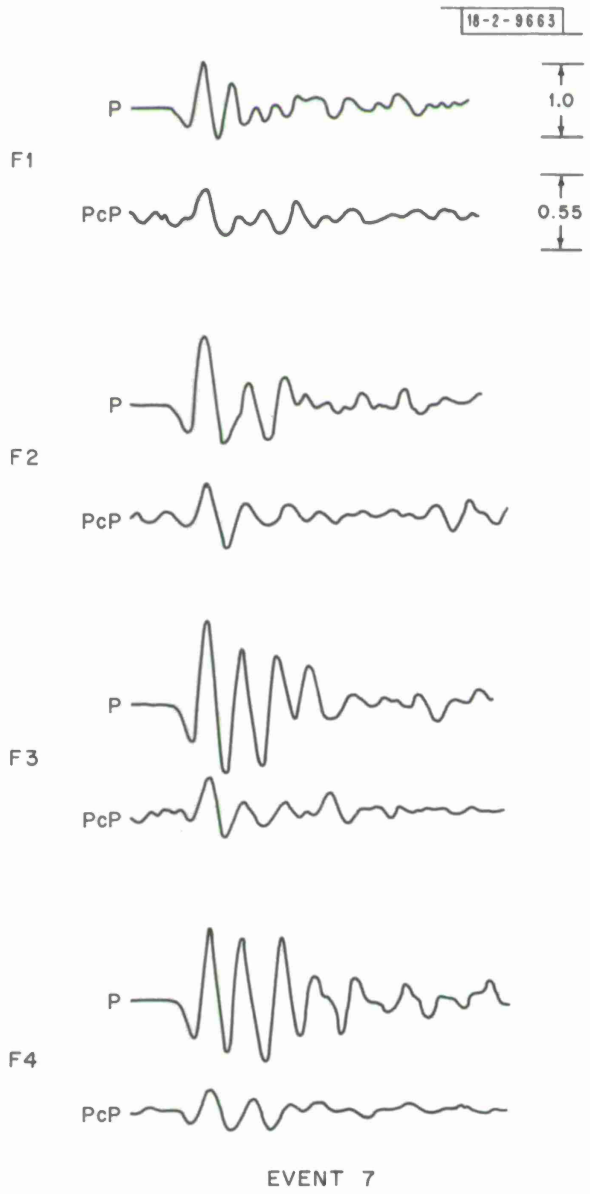

Fig. III-14. P and PcP phases for Kamchatka event, recorded on F ring at LASA.

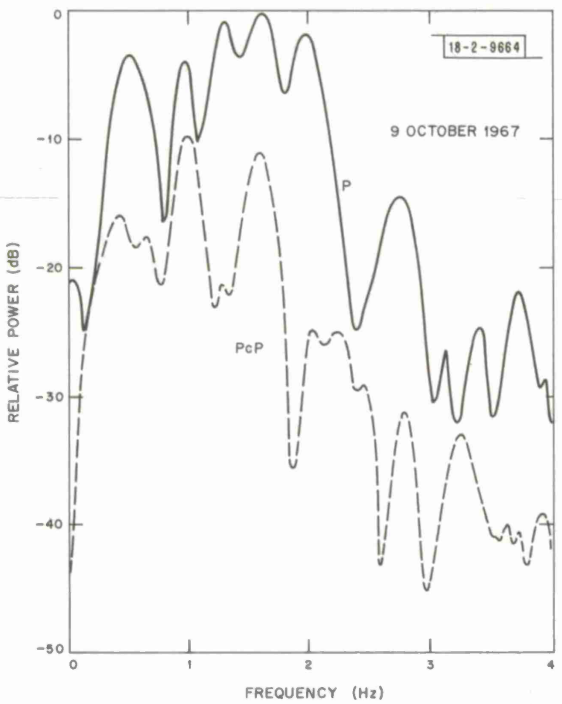

Fig. III-15. Amplitude spectra of P and PcP phases for Kamchatka event, recorded at F1.

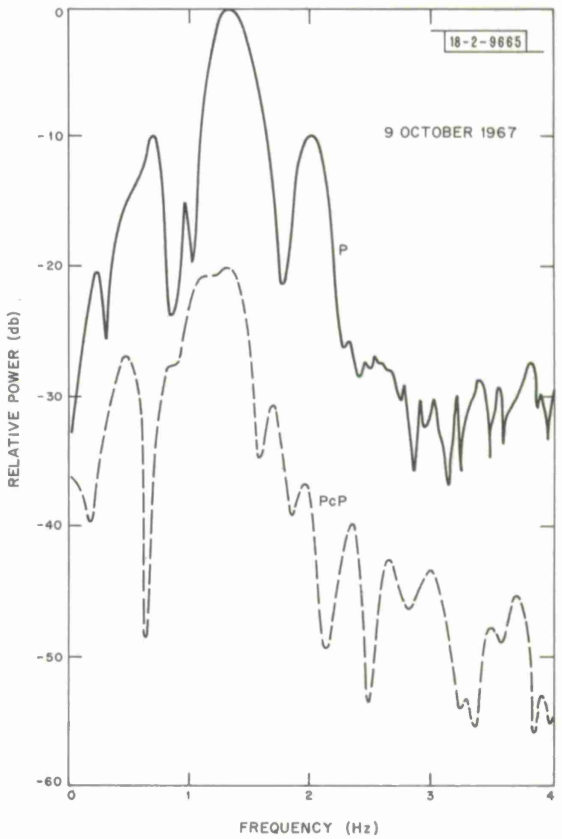

Fig. III-16. Amplitude spectra of P and PcP phases for Kamchatka event, recorded at F4.

IV. LINCOLN FACILITIES

A. DATA ANALYSIS CONSOLE

The Display program has been made more versatile by the addition of new commands that align the traces according to the time picks, move the display to a new time without turning the horizontal position knob, and allow the reference to be stored in the data base as another data channel. Some new programs have been added, in particular: Write TaPe (WTP), which outputs the entire data base onto magnetic tape in 'ffastro' format; Beamform from Azimuth and Velocity (BAV); and Beamform from Latitude and Longitude (BLL). These last two programs form beams steered for a plane wave of any incoming azimuth and velocity corresponding to an epicenter at any latitude and longitude.

In addition, the initializing has been generalized to allow these beamforming programs, as well as the location program, to work on any array of sensors. (Previously, they could only be used on LASA.) This is done by storing the latitude and longitude of each sensor on the drum for several standard arrays, e.g., NORSAR, UK sponsored arrays, TFO, ALPA. It is trivial to add more standard arrays.

P. L. Fleck
L. J. Turek

B. DAILY EPICENTER LOCATION BULLETIN

Since mid-1970 a daily epicenter location bulletin has been produced for use by group members in ordering LASA and NORSAR data. The daily bulletin covers a full 24-hour day and is available within 24 hours of the close of the day.

Seismic signals from the '10' seismometers in the F ring, D ring, and A0 and E3 subarrays are telemetered from Billings to Boston. The signals are filtered and recorded on three helicorders and one develocorder. Each working day an analyst will visually scan the develocorder output of the previous day and enter into a log the arrival times of all visible phases. These data are then placed on punched cards and input into a computer location program.

The computer program operates in a semi-automatic mode and allows some interaction on the part of the analyst. He can interact to restrain the distance, depth and number of stations used to locate the event. Prior to the final listing of epicenters the analyst can reject events which he feels are poorly located or have unacceptable station residuals. The final epicenter list is printed on computer paper and punched on paper tape suitable for teletype transmission.

A preliminary evaluation of the accuracy of the epicenter locations has been made using the Coast and Geodetic Survey list of preliminary epicenter locations as a reference. A bar graph of epicenter mislocations is shown in Fig. IV-1. The events used for this graph are in the 10° to 105° distance range. The large number of events with mislocations of 7° or more are probably due to events in the 95° to 105° distance range where location accuracy is known to be poor. This corresponds to events in the Philippine Islands, Solomon Islands and the Hindu Kush areas. Generally, about 75 percent of the locations are within three degrees.

The location threshold for events in the distance range of 20° to 60° can be determined from Fig. IV-2. This figure was obtained from plotting all events within this distance range that appeared on the bulletin. The upper curve represents the recurrence curve or total number of

located events equal to or greater than the given magnitude. The 90-percent cumulative threshold for events within this distance range is about magnitude 4.3. This means that locations for 90 percent of all events of magnitude 4.3 or greater will appear on the daily bulletin. The lower curve represents the total number of events actually reported in the bulletin. Figure IV-3 represents the same data for the distance range of 60° to 90°. For this distance range, the 90 percent cumulative threshold is at a magnitude of 4.4. These figures are consistent with a visual detection level at LASA of signals in the 3 to 4 mμ range.

R. M. Sheppard
L. C. Lande
Mary F. O'Brien

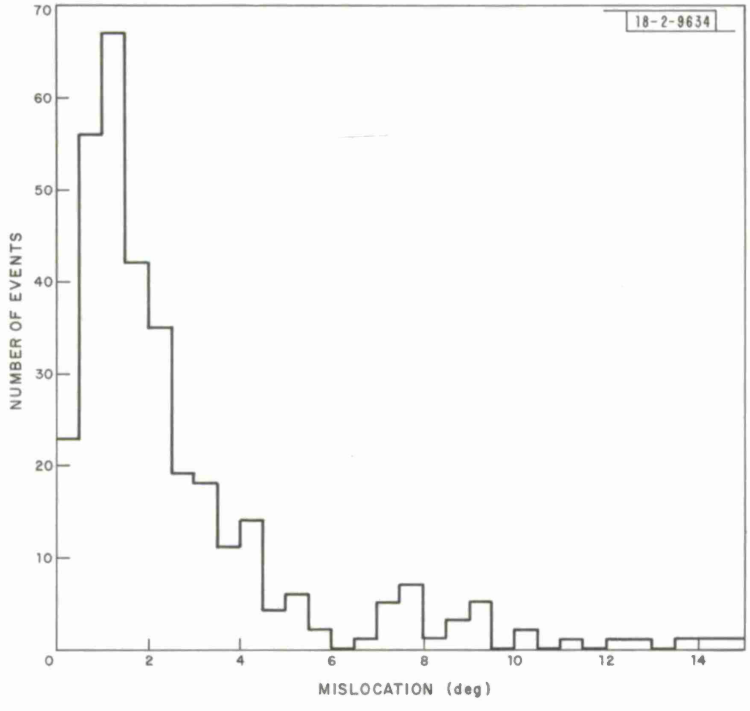

Fig. IV-1. Epicenter location accuracy.

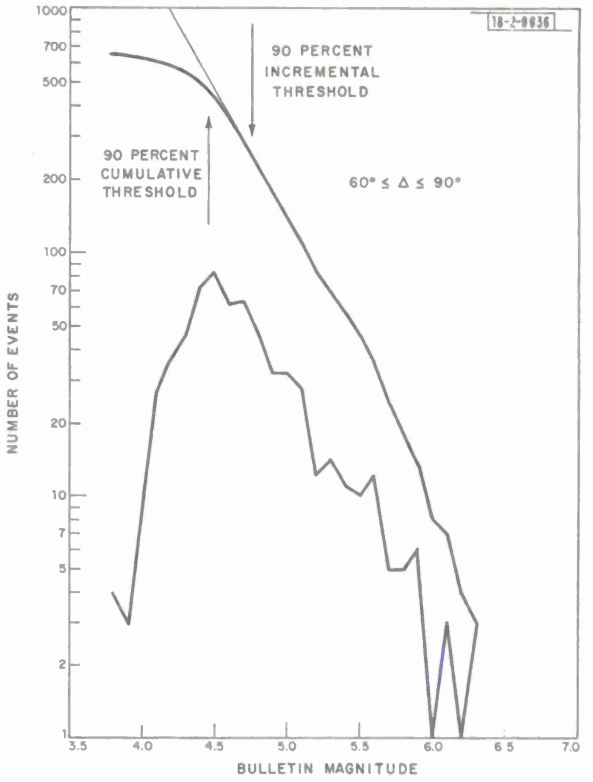

Fig. IV-2. Magnitude distribution of located events, $20° \leqslant \Delta \leqslant 60°$.

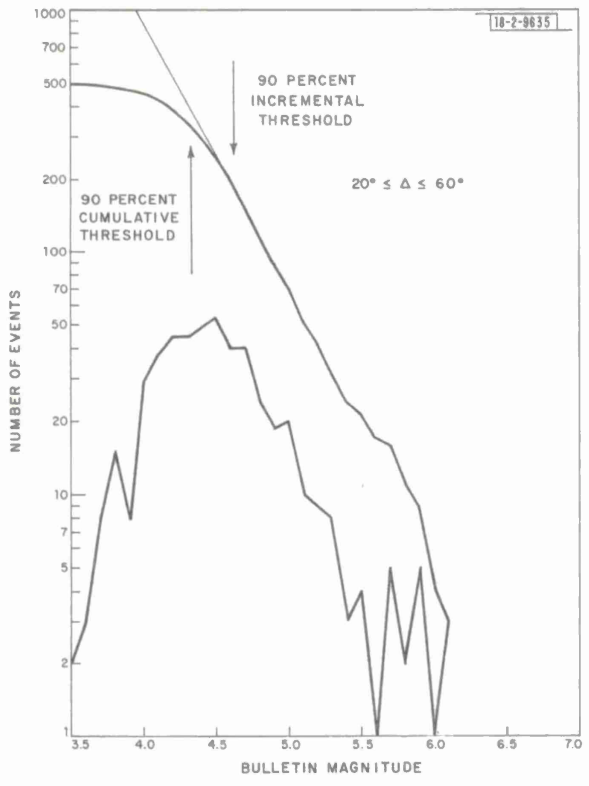

Fig. IV-3. Magnitude distribution of located events, $60° \leqslant \Delta \leqslant 90°$.

DOCUMENT CONTROL DATA – R&D

(Security classification of title, body of abstract and indexing annotation must be entered when the overall report is classified)

1. ORIGINATING ACTIVITY *(Corporate author)* Lincoln Laboratory, M.I.T.	2a. REPORT SECURITY CLASSIFICATION Unclassified 2b. GROUP None

3. REPORT TITLE

Seismic Discrimination, Semiannual Technical Summary Report to the Advanced Research Projects Agency

4. DESCRIPTIVE NOTES *(Type of report and inclusive dates)*
Semiannual Technical Summary Report - 1 July through 31 December 1970

5. AUTHOR(S) *(Last name, first name, initial)*

Davies, David

6. REPORT DATE 31 December 1970	7a. TOTAL NO. OF PAGES 68	7b. NO. OF REFS 39

8a. CONTRACT OR GRANT NO. F19628-70-C-0230 AF 49(638)-1763 b. PROJECT NO. ARPA Order 512 c. d.	9a. ORIGINATOR'S REPORT NUMBER(S) Semiannual Technical Summary 31 December 1970 9b. OTHER REPORT NO(S) *(Any other numbers that may be assigned this report)* ESD-TR-70-416

10. AVAILABILITY/LIMITATION NOTICES

This document has been approved for public release and sale; its distribution is unlimited.

11. SUPPLEMENTARY NOTES None	12. SPONSORING MILITARY ACTIVITY Advanced Research Projects Agency, Department of Defense

13. ABSTRACT

Research on source characteristics, propagation path effects and array processing is reported. The long-period characteristics of explosions are examined and tested against theoretical models. Short period worldwide data are used for a network study of a set of Eastern Kazakh events. A new computer program is being used to trace rays through heterogeneous structures. A detailed study of a Chinese event is given with particular reference to the impact that subsurface structure has on different discriminant tests. The spectraforming process is described and its impact on discrimination discussed. New facilities and the daily Lincoln bulletin are described.

14. KEY WORDS

seismic array seismometers seismology

Printed by
United States Air Force
L. G. Hanscom Field
Bedford, Massachusetts